The alteration history of the CY chondrites, investigated through analysis of a new member: Dhofar 1988

Suttle, M.D.[1] (*corresponding author*), Greshake, A.[2], King, A.J.[1,3], Schofield, P.F.,[1] Tomkins, A[4]., Russell, S.S.[1]
m.suttle@nhm.ac.uk, ansgar.greshake@mfn-berlin.de, a.king@nhm.ac.uk, p.schofield@nhm.ac.uk, andy.tomkins@monash.edu, sara.russell@nhm.ac.uk

[1.]Planetary Materials Group, Department of Earth Sciences, Natural History Museum, Cromwell Road, London, SW7 5BD, UK
[2.]Museum für Naturkunde, Leibniz-Institut für Evolutions und Biodiversitätsforschung, Invalidenstraße 43, 10115 Berlin, Deutschland
[3.]Planetary and Space Sciences, Open University, Walton Hall, Milton Keynes MK7 6AA, UK
[4.]School of Earth, Atmosphere and Environment, Melbourne, Victoria, Australia

Abstract

We provide the first detailed analysis of the carbonaceous chondrite Dhofar (Dho) 1988. This meteorite find was recovered in 2011 from the Zufar desert region of Oman and initially classified as a C2 ungrouped chondrite. Dho 1988 is a monomict breccia composed of millimetre-sized clasts, between which large (~50-250µm) intermixed sulphide-Ca-carbonate veins formed. It has high sulphide abundances (~14 vol%), medium-sized chondrules (avg. 530µm, N=33), relatively low chondrule/CAI abundances (<20 area%), a heavy bulk O-isotope composition ($\delta^{17}O$=9.12‰, $\delta^{18}O$=19.46‰) and an aqueously altered and then dehydrated alteration history. These characteristics are consistent with the newly defined Yamato-type (CY) carbonaceous chondrite group, suggesting this meteorite should be reclassified as a CY chondrite.

Dho 1988 experienced advanced aqueous alteration (petrologic subtype 1.3 in the scheme of Howard et al., [2015]). Alteration style and extent are similar to the CM chondrite group, with the matrix having been replaced by tochilinite-cronstedtite intergrowths and chondrules progressively pseudomorphed by phyllosilicates, sulphides and in one instance Ca-carbonates. However, departures from CM-like alteration include the replacement of chondrule cores with Al-rich, Na-saponite and upon which Cr-spinel and Mg-ilmenite grains precipitated. These late-stage aqueous alteration features are common among the CY chondrites. Fractures in Dho 1988 that are infilled by phyllosilicates, sulphides and carbonates attest to post-brecciation aqueous alteration. However, whether aqueous alteration was also active prior to brecciation remains unclear. Veins are polymineralic with a layered structure, allowing their relative chronology to be reconstructed: intermixed phyllosilicate-sulphide growth transitioned to sulphide-carbonate deposition. We estimate temperatures during aqueous alteration to have been between 110ºC<T<160ºC, based on the co-formation of Na-saponite and tochilinite. Dho 1988 was later overprinted by thermal metamorphism. Peak temperatures are estimated between 700ºC and 770ºC, based on the thermal decomposition of phyllosilicates (both serpentine and saponite) combined with the survival of calcite. As temperatures rose during metamorphism the thermal decomposition of pyrrhotite produced troilite. Sulphur gas was liberated in this reaction and flowed through the chondrite reacting with magnetite (previously formed during aqueous alteration) to form a second generation of troilite grains. The presence of both troilite and Ni-rich metal in Dho 1988 (and other CY chondrites) demonstrate that conditions were constrained at the iron-troilite buffer.

***Keywords**: Asteroids, CY chondrites, thermal metamorphism, aqueous alteration*

1. Introduction

Carbonaceous chondrites are some of the most primitive extraterrestrial materials available for study. Their chemical compositions and accretionary mineral assemblages preserve signatures of the protoplanetary disk from which they formed (Ebel et al., 2016; Braukmüller et al., 2018; Gregory et al., 2020), while their later alteration histories record the geological activity that operated on small bodies in the early solar system (Lee et al., 2012; King et al., 2017).

There are eight (sub-)groups of carbonaceous chondrite currently recognised (Weisberg et al., 2006). These divisions are based on distinctive bulk chemical and oxygen isotope compositions as well as primary petrographic characteristics that relate to their accretionary history (e.g. chondrule and Ca, Al inclusion [CAI] sizes and abundances). Historically, each chondrite group was thought to represent a separate parent body (Weisberg et al., 2006). However, groupings could instead represent a series of closely related bodies (Greenwood et al., 2019; 2020; Gattacceca et al., 2020) that formed within a single chemically/isotopically homogenous region of the protoplanetary disk. Complicating the picture further, in addition to the established groups, there are numerous ungrouped meteorites (Choe et al., 2010) whose significance remains unresolved. Some have properties intermediate between groups, as in the case of several ungrouped C2 meteorites (e.g. Adelaide, NWA 5958 and Acfer 094) that span the CO-CM gap (Greenwood et al., 2019). The presence of intermediate ungrouped meteorites presents problems for a simplistic "*one parent body per group*" interpretation and instead implies that that chondrite groups could reflect different reservoir regions in the early protosolar nebula.

The analysis of secondary minerals (those formed on the parent body after accretion) and alteration textures provide insights in the geological evolution of small bodies. The alteration histories of asteroids are complex but often involve interaction between primary phases and liquid water, a process termed aqueous alteration (Bischoff, 1998). In addition to fluid interaction, many chondrites also preserve evidence of thermal metamorphism, attesting to relatively high-temperature solid state and metasomatic reactions (Nakamura, 2005). Impact events resulting in shock deformation, shock heating and phase transitions were also common in the early solar system and their effects are likewise recorded in deformed meteorites (Lindgren et al., 2015). In this study we explore a previously undescribed carbonaceous chondrite: Dhofar (Dho) 1988. This meteorite bears a resemblance to the properties of the recently defined Yamato-type (CY) carbonaceous chondrite group (Ikeda, 1992; King et al., 2019). As such we decided to perform a detailed investigation of its mineralogy and petrography to determine its origin, parent body affinities, alteration history and relationship to the CYs.

2. The CY chondrites

The CY chondrites are a collection of meteorites that potentially represent the ninth carbonaceous chondrite group (King et al., 2019). Investigation in the late 1980's by an international consortium suggested that the "*Belgica Grouplet*" (Belgica-7904, Y-82162 and Y-86720) should be reclassified as the CY chondrites (Ikeda 1992). However, the CY nomenclature was not widely adopted by the community. More recently, King et al., (2019) reanalysed the same meteorites along with several other closely related Antarctic specimens and re-proposed the CY chondrite term, supporting the original conclusions of Ikeda (1992). They have clear petrographic, geochemical and isotopic links as well as a shared parent body alteration history (Ikeda, 1992; King et al., 2019). The basic properties of this (potential) meteorite group are outlined below.

2.1. Primary characteristics: Major element bulk chemical data for CY chondrites is shown in Ikeda (1992 [Table.5]) and King et al., (2019 [Table.A1]). They typically have chemical compositions intermediate between the CI and CM chondrites (Paul and Lipschutz, 1990). Several members have bulk compositions closer to CI values and were originally classified as CI chondrites (Y-82162, Y-86029

and Y-980115 [Tomeoka et al., 1989a; Ikdea, 1991; Tonui et al., 2002; Kikuchi et al., 2015]). In contrast, other members (such as B-7904 and Y-86720) have compositions more similar to CM chondrites and in the past have been classified as anomalous CMs (Tomeoka et al., 1989b; Yamamoto and Nakamura 1990). Average major element abundances vary by less than one order of magnitude from CI values and are characterised by minor depletions in refractory elements with CI-like or mildly enriched concentrations of moderately volatile elements. The CY chondrites also have distinctive trace element compositions. Their rare earth elements (REEs) display a light/heavy fractionation trend (Yamamoto and Nakamura 1990) while thermally mobile trace elements (Ce, Se, Ag, Te, Zn, In, Bi Tl and Cd) have pronounced depletions, relative to CI chondrites (Paul and Lipschutz, 1990; Tonui et al., 2002; 2014; Braukmüller et al., 2018; King et al., 2019). These trace element signatures are interpreted as a product of thermal metamorphism resulting in the loss of volatile-bearing chalcophile-rich fluids.

Currently, chondrule and CAI data for the CY group is limited. Although several publications have analysed individual CY meteorites in detail, published data on chondrules and CAIs have often been grouped together, and so an assessment of their individual relative abundances and size distributions has not been possible. We have summarized the literature data on CY meteorites in Table.1. The average chondrule size in CY chondrites (~420µm) is larger than that found in CO and CM chondrites (~150µm and 300µm respectively [Weisberg et al., 2006]) but smaller than the CV and CR chondrite averages (1000µm, and 700µm respectively [Weisberg et al., 2006]). Maximum chondrule sizes in the CY chondrites exceed 1000µm and (up to 3000µm, Bischoff and Metzler, 1991). Combined chondrule/CAI abundances are <26 area% and average ~18 area% (Table.1). The abundance of fine-grained matrix in the CYs is therefore similar to that found in CM chondrites (20 vol%, Weisberg et al., 2006). It should also be noted that three CYs (Y-82162, Y-86029 and Y-980115) are reported to preserve neither chondrules nor CAIs and thus have textures similar to the CI chondrites, being composed of ~100% fine-grained matrix (Tomeoka et al., 1989a; Tonui et al., 2002; Kikuchi et al., 2015).

One of the defining primary characteristics of the CY chondrite group are their uniquely heavy bulk oxygen isotope compositions. These were first reported by Clayton and Mayeda (1999), who analysed B-7904, Y-82162, Y-86720, and Y-86789 and noted that they have the highest $\delta^{17}O$ and $\delta^{18}O$ compositions yet measured in meteorites. The average CY bulk O-isotope composition lies at approximately $\delta^{17}O$: +10.3‰, $\delta^{18}O$: +21.2‰ and $\Delta^{17}O$: -0.7‰ (Fig.1). This is distinctly outside the ranges of all established chondrite groups, further justifying their treatment as a separate group. Interestingly if the CO-CM O-isotopic mixing line is extended to heavier compositions, the CY chondrites are found to plot directly on this line (Fig.1), with the same slope function (0.7) and $\delta^{17}O$ intercept (-4.23‰). The CO-CM mixing line is best explained as a product of mixing between two early isotopic reservoirs: an inner ^{16}O-rich solar-like silicate reservoir upon which additions from a cold outer ^{18}O-rich volatile water-ice component were added (Clayton and Mayeda, 1999; Alexander et al., 2018). The measured bulk O-isotope composition of the CY chondrites will be both a product of their initial formation mechanisms and later parent body alteration effects shifting their values to heavier compositions (Clayton and Mayeda, 1999; King et al., 2019).

A notable feature of the CY chondrites that distinguishes them from the CM and CI chondrites is their remarkably high sulfide contents (~20vol%, King et al., 2015a; 2019). Based on modal mineralogy the CYs have phyllosilicate/sulfide abundance ratios between 2 and 5. This is in stark contrast to the average values between 15 and 40 for the CM and CI chondrites, respectively. Such high sulfide contents necessarily require a significantly higher sulfur budget. The abundant S-bearing minerals in CYs are dominated by pyrrhotite and troilite, with trace pentlandite and Cu-sulfides (cubanite) (Tomeoka et al., 1989a; Ikeda, 1991). These sulfide minerals have a wide range of morphologies, including large euhedral laths (>400µm) (King et al., 2019), as well as fine grains closely associated with the phyllosilicates (Bischoff and Metzler, 1991).

2.2. Parent body alteration history of the CY chondrites: The CY chondrites experienced significant interaction with liquid water on their parent body(ies) resulting in the formation of widespread

hydrated minerals including phyllosilicates and tochilinite (Tomeoka et al., 1989b; Akai, 1990; King et al., 2019). Later, thermal metamorphism overprinted the effects of aqueous alteration. The CY chondrites are therefore dehydrated meteorites with metamorphic mineral assemblages. Prior to their recognition as thermally metamorphosed, they were considered hydrated and assigned either C2 or C1 petrologic subtypes (Ikdea, 1992; King et al., 2019). This is largely because the CY chondrites contain fibrous and flake-like phases dispersed throughout their matrix and such textures are typical of phyllosilicates. These phyllosilicate-like textures are, however, pseudomorphs produced by the solid-state recrystallization of phyllosilicate into olivine (and termed secondary olivine hereafter). Solid-state reactions can preserve both the textures and to a lesser extent the chemical composition of their former phases (Akai, 1992; Suttle et al., 2017). Replacement reactions like these occur when hydrated materials are heated above ~400ºC and have been reported in both chondritic meteorites (e.g. Nakamura, 2006; Tonui et al., 2014) and flash heated micrometeorites (Suttle et al., 2017; 2019). Analysis of the metamorphosed minerals in CYs therefore allows a partial reconstruction of their former hydrated mineral assemblage. The inferred phyllosilicates in CY chondrites were most likely a mixture of both serpentine and saponite, as suggested by their cation chemistry plotted in ternary diagrams (Akai, 1990; Tomeoka, 1990). The CY matrix also retains anomalously high Na contents (~2wt.% Na_2O in B-7904, Lipschutz et al., 1999 and 1.4-4.6wt.% Na_2O in Y-82162, Tomeoka et al., 1989a), leading several researchers to suggest that Na-bearing phlogopite, Na-talc or Na-chlorite were minor components of the (previously) hydrated matrix (Tomeoka et al., 1989a; Ikeda, 1991; Tonui et al., 2002).

The later episode of thermal metamorphism resulted in the near-complete dehydration and subsequent recrystallization of matrix phyllosilicates. The hydrated matrix was replaced with an intermixed groundmass composed of dehydroxylates (phases formed by the loss of structural OH molecules from phyllosilicates [Nozaki et al., 2006; Che and Glotch 2012]) and recrystallized micron-size secondary olivine forming a groundmass (Akai, 1990; 1992). The CYs have 5-10 wt.% H_2O in Y-82162 and Y-980115, <5 wt.% in Y-86720 and B-7904 (Tomeoka et al., 1989a; 1989b; Lipschultz et al., 1999; King et al., 2015a), and 1.0-1.8wt.% in Dho 225 and Dho 735 (Ivanova et al., 2010). The duration of heating affecting the CYs may have been relatively short, as inferred from Fe-Mg zoning profiles in primary mafic silicates (10-1000 days, Nakato et al., 2008), from experimental studies on the thermal decomposition of carbonates (Kikuchi et al., 2015), and from the noble gas budget of Y-980115 (~100 minutes, Kikuchi et al., 2015). Thermal metamorphism may have also affected the group's bulk O-isotope composition, shifting to heavier (^{16}O-poor) values (Clayton and Mayeda, 1999; Nakamura, 2005; Ivanova et al., 2013).

The CY modal mineralogy, as determined by X-ray diffraction (XRD, Schofield et al., 2002; Howard et al., 2009), is dominated by thermally decomposed phyllosilicates. These are now present either as highly disordered dehydroxylates or as recrystallized secondary olivine. Combined, these phases average 70 vol%, varying between 58-79 vol% (King et al., 2019). The next most abundant phases are Fe-sulfides (between 12-29 vol%, avg. 21 vol%), with variable quantities of primary anhydrous silicates (0-20 vol% olivine and/or 0-11 vol% pyroxene). Minor phases detected by XRD include magnetite (<5 vol%) and FeNi metal (<2 vol%) (King et al., 2015a; 2019). Under Scanning Electron Microscope (SEM) the CYs also contain several exotic accessory phases (at <1 vol%), including a diverse array of Mg-Fe-Ca-Mn-carbonates such as, breunnerite, magnesite, dolomite and rhodochrosite [Ikeda, 1992]), Ca-phosphates (whitlockite and apatite), Cu-Fe sulphides, Na-bearing phyllosilicates (now as dehydroxylates), ilmenite-bearing Al-rich inclusions (Bischoff and Metzler, 1991) and Mn-bearing periclase ([Mg,Fe]O, Tomeoka et al., 1989a; 1989b; Tonui et al., 2002; King et al., 2019).

2.3. Members of the CY group: Currently, the CY group includes: Yamato (Y)-82162 [C1/2-ung], Y-86029 [CI1], Y-86720 [C2-ung] paired with Y-86789 [C2-ung], Belgica (B)-7904 [C2-ung] and Y-980115 [CI1]. Additional potential members of non-Antarctic origin could include: Dhofar [Dho] 225 [CM-an], Dho 735 [CM2] (Ivanova et al., 2010), Dho 955 [CM2] (Russell et al., 2005; Ivanova et al., 2005), Dho

2046 [CM2-an] (Bouvier et al., 2017a), Dho 2066 [C-ung] (Gattacceca et al., 2019) and the subject of this study, Dho 1988 [C2-ung] (King et al., 2019).

3. The subject meteorite: Dhofar 1988

Dhofar 1988 is a meteorite find recovered from the Zufar desert region of Oman on 02/12/2011 at co-ordinates 19°4.865'N, 54°46.024'E and with a total mass of 59g. This sample was reported in the 104th issue of the Meteoritical Bulletin (Bouvier et al., 2017b) where it was classified as C2 ungrouped (C2-ung), with S1 shock (unshocked). The meteorite was originally described as a breccia with a grey to dark black interior, containing clearly resolvable chondrule pseudomorphs (with a mean average diameter of 550µm) and rare mineral grains set in a matrix of phyllosilicates, Ca-carbonates and sulphides. Anhydrous silicates were found to be exclusively olivine, generally with high-Mg compositions (Fa1.6±0.8 [n=77]). Dho 1988 has a low degree of terrestrial weathering. Bulk oxygen isotope compositions from acid-washed replicate analyses under laser fluorination gave: $\delta^{18}O$=16.4‰, 21.9‰, 20.1‰; $\delta^{17}O$=7.0‰, 10.8‰, 9.6‰; $\Delta^{17}O$= -1.6‰, -0.8‰, -1.0‰ (relative to Vienna Standard Mean Ocean Water [VSMOW]) (Bouvier et al., 2017b).

4. Methods

In this study we analysed both a polished thin section (MNB-XV-II-36) and a ~73mg fusion-crust free chip (MNB-MET-6709) of Dho 1988 loaned from the Museum für Naturkunde, Berlin. The section has a total area of 62mm^2 and was used for non-destructive microanalysis by SEM, while the chip was powdered and used for bulk measurements and destructive studies, including XRD analysis to determine modal mineralogy and thermogravimetric analysis (TGA) to estimate the sample's volatile content. Analyses were performed at the Natural History Museum (NHM), London.

4.1. SEM-EDS-WDS analyses: The thin section was analysed using backscatter electron (BSE) imaging, (quantitative) standards-based energy dispersive X-ray spectrometry (EDS) and high-spatial resolution X-ray elemental mapping using a Zeiss EVO 15LS SEM fitted with an Oxford Instruments' 80mm^2 X-Max silicon drift detector (SSD) energy dispersive spectrometer. All EDS analyses were performed under high-vacuum and at a fixed working distance of 8.5mm. An electron beam accelerating voltage of 20kV and beam current of 1.5nA were used, resulting in an output count rate of approximately 40-60kcps for silicate minerals. Spot analyses were acquired with a 5s acquisition time and ~30% deadtime. Throughout the analysis the beam current was monitored at regular intervals using the built-in Faraday cup. Prior to analysis, the EDS system was calibrated (for gain and energy channel) using a polished cobalt metal standard and the resulting EDS data processed using the Oxford Instruments Aztec software. Standards-based quantification was performed using calibrated reference samples and applying standard XPP matrix correction routines (Wendt and Schmidt, 1978). For silicate minerals, weight total were determined using the "*oxygen by stoichiometry*" quantification routine, while for carbonate minerals we used the "*carbon by difference*" routine and for sulphides and metals we used the "*all elements*" routine. The accuracy and precision for major rock-forming silicate cations were cross-checked against analyses on the Smithsonian Kakanui augite reference standard, whose composition is known from dissolution. Element detection limits are on the order of 0.1-0.3wt.%, while analytical uncertainties have a relative error dependent on the element's concentration. For major elements (>10wt.%) uncertainties are 1-3wt.%, for minor elements (>2-10wt.%) uncertainties vary by 0.1-1.0wt.% and for trace elements (<2wt.%) uncertainties are 0.05-1.0wt.%.

We also collected a whole-section EDS map, produced by montaging 255 fields, each with a size of 252x189 pixels (approx. 555µmx415µm=0.23mm^2), translating to a spatial resolution of ~1.9µm/px. This map was collected at 20kV, with a higher beam current of 3nA, leading to increased output count rates (>50kcps) and higher deadtimes (varying between 30-60%). Each frame had a live acquisition

time of approximately 270s. Combined element maps are shown in Fig.2 while single element maps are displayed in Fig.S1.

Additional BSE imaging and geochemical analyses were conducted at the Museum für Naturkunde, Berlin using a JEOL JXA 8500F field emission cathode electron microprobe equipped with five wave dispersive spectrometry (WDS) spectrometers applying 15 kV accelerating voltage, a 15 nA beam current, and 1-5 µm beam sizes. Suitable mineral standards including anorthoclase, basaltic glass, chromite, chromium augite, diopside, ilmenite, microcline, and plagioclase, all certified by the United States National Museum of Natural History as reference samples for electron microprobe analysis (Jarosewich et al., 1980) were applied to calculate mineral compositions.

4.2. XRD: Approximately 50mg of the powdered aliquot was analysed with an ENRAF Nonius FR 590 X-ray diffractometer fitted with a curved 120° position sensitive detector (PSD-XRD). Following conventional operation protocol (identical to that in King et al., 2015a; 2019), copper Kα1 radiation was selected using a Ge 111 monochromator. The beam footprint upon the powdered sample was set using post-monochromator slits at 0.24x2mm. X-ray diffraction patterns were collected for 16 hours from the meteorite sample and for 30 minutes for each of the pure mineral standards. After phase identification, modal mineralogy was calculated using a profile-stripping method that has previously been applied to >50 carbonaceous chondrites at the NHM (Bland et al. 2004; Howard et al. 2009; 2012; 2015; King et al. 2015; 2017; 2019). Profile-stripping is achieved by scaling the mineral standard patterns and then reducing their intensities by a given factor until a match is achieved against the relevant features within the meteorite's pattern. The mineral standard patterns are then subtracted from the meteorite's, leaving a final residual pattern with (approximately) zero counts. Finally, the fit factors for each mineral standard are corrected against their relative differences in X-ray absorption to produce volume fraction estimates for each phase within the meteorite (Cressey and Schofield 1996). In general, modal abundances are limited to phases present at ≥0.5 vol%.

4.3. TGA: Approximately 13mg of Dho 1988 (taken from the XRD powder) was analysed using a TA Instruments SDT Q600 TGA at the NHM. The powdered meteorite was held in an alumina crucible and heated inside a continuously flowing N_2 atmosphere with a flow rate of 100mlmin^{-1}. Volatile loss was measured as a change in mass per temperature step (wt%/°C) as the sample was heated from room temperature (17°C) to 1000°C at a heating rate of +10°Cmin^{-1}. The sensitivity of our TGA balance is 0.1µg and the overall error on the measured mass loss fractions is approximately 0.1%. The resulting mass-temperature curve illustrates the rate of mass loss as a function of temperature. Since different phases within carbonaceous chondrites undergo thermal decomposition over distinct temperature ranges, the measured mass loss at each temperature window provides important information regarding both which phases contained water, (or other volatiles) and what fraction of these volatiles were lost (Garenne et al., 2014; King et al., 2015b).

Previous studies have demonstrated that aqueously altered carbonaceous chondrites release adsorbed terrestrial water at temperatures <200°C, water from Fe-(oxy)hydroxides between 200–400°C (Garenne et al., 2014), water from phyllosilicates between 350–800°C (Akai, 1992; Nakamura, 2005; Nozaki et al., 2006; Che and Glotch, 2011; 2012) and finally CO_2 from the breakdown of carbonates is released between 770–900°C (Greshake et al, 1998). Additionally, Fe-sulphides release S-bearing volatiles between approximately 400-650°C (Burgess et al., 1991; Garenne et al., 2014).

5. Results

5.1. Petrography: Dho 1988 (Fig.2) has a high abundance of matrix (~60-70 area%) and correspondingly a low abundance of coarse-grained chondrules and CAIs (~20 area%). The remaining

10-20 area% in Dho 1988 is predominantly sulphides and carbonates. The mineralogy of Dho 1988 is dominated by the products of both aqueous alteration and thermal metamorphism.

Chondrules are well-defined and vary in (apparent) diameter up to a maximum value of 2330µm. Mean chondrule sizes are 530µm, with a median value of 350µm (N=33). Most are partially altered or pseudomorphs entirely replaced by phyllosilicates (subsequently dehydrated), although some minimally altered chondrules survive (Fig.3). We identified a single pseudomorphic chondrule in which the entire assemblage (and surrounding fine-grained rim) has been replaced by a mixed carbonate-sulphide secondary mineralogy (Fig.3F). Inferred chondrule textures are predominantly porphyritic types with some coarse-grained and single crystal varieties. Most chondrules have multi-layered fine-grained rims with Fe-rich compositions (Table.2), others have "*armoured*" textures characterised by an outer sulphide-rich mantle.

Texturally, Dho 1988 is a partially lithified clast-supported monomict breccia composed of millimetre-sized clasts each derived from the same lithology and separated by mineralized veins (Fig.2D). Clasts vary significantly in texture, some are nearly chondrule-free and instead composed principally of fine-grained matrix while others are chondrule-rich as seen in the whole section images (Fig.2). Clasts are separated by cracks of variable length and width which have been infilled by an intermixed mineral assemblage forming veins composed of (former) phyllosilicate with carbonate and sulphide.

Primary anhydrous silicates are overwhelmingly high-Mg olivine with compositions between Fo81.0-99.7 and a mean average value of Fo97.4 (±3.2, N=91, Fig.4A). They are most commonly found within partially altered chondrule cores but are also present as large (>100µm) isolated grains within the matrix. Chondrule olivine occasionally contains poikilitic metal droplets with kamacite compositions. In addition, we identified a single chondrule with more Fe-rich composition (Fo74.0-83.5) and a zoned texture (Fig.3B). Pyroxene occurs as enstatite grains with a small, rounded appearance and located at the margins of (partially altered) POP chondrules. They contain anomalously high Al contents (Table.2, avg. Al ~2.24wt.% [±0.52wt.%]) and have non-stochiometric compositions, with low silicate abundances under EDS/WDS analyses. These pyroxenes have virtually no Ca and are thus members of the orthopyroxene solid solution. They have Mg# between 54-79 and average values of 72.8 (±6.3, N=49).

According to our analyses, Dho 1988 contains no hydrated phyllosilicate, despite much of the sample's matrix being dominated by phases with textures almost identical to the phyllosilicate-rich matrix of hydrated carbonaceous chondrites (Figs.1, 2, 4 and Table.2 rows labelled as "2nd ol."). They produce high analytical weight totals (~91wt.%) when analysed under SEM-EDS/WDS and have abundant dehydration cracks (as seen in BSE images [e.g. Fig.5F]), features that are inconsistent with a hydrated composition. Instead these features are evidence of thermally processed phyllosilicates in which dehydration followed by recrystallization occurred as solid-state reactions resulting in secondary olivine which preserves its former phyllosilicate texture (Suttle et al., 2017).

Although phyllosilicates no longer exist, their former textures, relative abundance and composition can be reconstructed by analysing the secondary olivine grains that replaced the phyllosilicates (Fig.4 and Table.2). Two main species of (former) phyllosilicate are distinguishable by texture and geochemistry.

(1) The dominant form is a fine-grained Al-poor species (on average: 1.56 ±0.77wt.% and whose Mg# varies between 36-93 with an average value of 69 (±11)). Much of the meteorite's matrix would have been composed of these phases. Spot analyses show variable quantities of Fe, Ni and S (Fig.4C), consistent with the presence of small FeNi-sulfide grains intermixed with the (former) phyllosilicate. Therefore, before thermal metamorphism, the matrix of Dho 1988 was most likely composed of tochilinite-cronstedtite intergrowths (TCIs), similar to those found in CM2 chondrites (e.g. Tomeoka et al., 1989c; Lauretta et al., 2000).

(2) The other (inferred) phyllosilicate phase was present within the altered chondrule cores. This species was coarser-grained and had higher Al contents (about 2-11wt.%) (Fig.4C). These Al-rich

former phyllosilicates would have had lower concentrations of most cations (e.g. Ni, Cr, Mn and Ti) but variable Na contents that extend up to values of ~1.8wt.%. They are coated by a thin mantle of micron-sized refractory metal oxides (Fig.5D and E), i.e., Cr-spinels with Cr contents between 20-52wt.% and Mg-bearing (<4wt.%) ilmenite grains. Both of the former phyllosilicate species have abundant dehydration cracks, which have been infilled by Fe-sulphide grains (Fig.5G).

Plotting the cation compositions of the secondary olivine on a Si-Fe-Mg ternary diagram (Fig.4B) allows the approximate composition of their phyllosilicate precursors to be reconstructed. This suggests that both species were members of the serpentine group with compositions near the Mg-serpentine endmember. Saponite was therefore not common.

Throughout Dho 1988 sulphur almost exclusively takes the form of low-Ni (<6wt.% and typically <1.7wt.%) troilite, while tochilinite is absent. Within an altered chondrule core we also identified a single irregular mass composed primarily of Fe, Cr and S (Table 1) with an approximate stoichiometry of $(Cr,Fe)_5S_4$ and a low total that may suggest partial oxidation.

Vein mineralogy is dominated by irregular-shaped calcite masses, hosting abundant subhedral Fe-sulphide (troilite) grains (Fig.5A). They have heterogenous textures with localised regions containing coarse-grained troilite crystals (>50µm) as grain clusters (approximately 10-40 grains) held within a well-developed homogenous carbonate host. These coarse-grained regions are separated from each other by porous fine-grained material composed of intermixed micron-sized carbonate and sulphide. Rare irregular-shaped Cl-F-bearing hydroxy-apatite grains (containing F at 1.49wt.% [±0.67] and Cl at 0.51wt.% [±0.23]) with anhedral morphologies and grain sizes <20µm are also found within the Ca-carbonate host (Fig.5C). At the vein walls darker low porosity regions are seen in BSE images (Fig.5 and S2). Based on correlated Al, Si, Mg, Fe and S they appear to be (former) phyllosilicates interspersed with Fe-sulphides (Fig.S2). Carbonates are also found within the silicate clasts, forming a network of thin (<5µm) veins. These carbonates have homogenous textures and do not contain embedded sulphides. In places they are seen to have infilled the dehydration cracks of (former) phyllosilicates.

Carbonates in Dho 1988 include large veins, small veins and the single carbonate chondrule. All these morphologies have remarkably similar major and minor element chemical compositions, as indicated by the small standard deviation values given in Table.2.

5.2. Modal mineralogy: Crystalline phases identified in the meteorite's bulk XRD pattern (Fig.6, Table.3) include olivine, pyroxene, troilite and calcite. Characteristic diffraction peaks from phyllosilicates were not detected. The most abundant phase is olivine at 73 vol%, followed by Fe-sulphides (exclusively troilite) at 14 vol%. Pyroxene, and calcite occur as relatively minor phases at 7 vol% and 5 vol%, respectively. The olivine component represents the sum of both primary olivine (at 11 vol%) of nebula origin and secondary olivine (at 62 vol%) formed by the thermal decomposition and subsequent recrystallization of former phyllosilicates (Akai, 1990; 1992; Nozaki et al., 2006; Che and Glotch, 2011; 2012; Suttle et al., 2017). The presence of both primary and secondary olivine in thermally metamorphosed carbonaceous chondrites is common and resolvable from XRD data (see Fig.A1 in King et al., 2019). Primary olivine has sharp diffraction peaks, while secondary has much broader peaks due to its low crystallinity and fine grain size. Furthermore SEM-EDS data supports this dichotomy showing that primary olivines (commonly found in partially altered chondrule cores) have high-Mg compositions >Fo90, while secondary olivines have low-Mg compositions of Fo_{50-90} (Table.2 & Fig.4A).

5.3. TGA: Dho 1988 experienced 2.72wt.% mass loss over the temperature range 200-770°C (Fig.7). This decrease is significantly lower than the mass loss experienced by hydrated CM, CR and CI chondrites (which average ~10-14wt.%, 7-15wt.% and ~20wt.%, respectively Garenne et al., 2014; King et al., 2015b). By contrast, the nominally anhydrous CV chondrites lose between 0.4wt.% and 9.9wt.% (with an average value of 4.7wt.%) over the temperature range 200-900°C (Bonal et al., 2020).

Dho 1988 exhibits two main volatile mass loss events (seen as peaks in the derivative thermogravimetry [DTG] curve [Fig.7]) at approximately 350°C and 660°C. The lower temperature (350°C) peak is less pronounced and has an asymmetric profile, skewed towards higher temperatures, meanwhile the main peak (at 650°C) is symmetric and significantly larger (equating to a more significant mass loss event, Fig.7). The positions of both peaks correlate well with the positions of peaks from our troilite mineral standard (BM1923, 21) heated over the same range (and on the same instrument). This confirms that (at least some of) the volatile loss from Dho 1988 is due to the thermal decomposition of troilite, with gas loss occurring as sulphur. However, because the relative intensities of the two peaks in the Dho 1988 analysis do not match well with the relative intensities of the troilite standard this suggests that the breakdown of an additional phase also contributed to the higher temperature (660°C) peak in the Dho 1988 analysis. The decomposition of calcite is likely to have contributed to the volatile gas budget (TGA curves for calcites are shown in Fig.S3). Calcite decomposes at temperatures between 600-900ºC, releasing CO_2. Although our internal calcite standard has a decomposition peak located at ~760ºC, the exact temperature of break-down depends on grain size, crystallinity and cation composition (Salvador et al., 1989).

Taking these observations together allows the quantity of water in Dho 1988 to be evaluated. Troilite loses just 2.5% of its weight on heating between 0-1000ºC (Fig.7). The XRD data suggests Dho 1988 contains 14 vol% troilite (equivalent to ~20wt.% troilite). Assuming all the troilite decomposed this would result in a mass loss of just 0.5wt.%. Conversely, calcite loses 44% of its mass during thermal decomposition to CaO. If all the calcite in Dho 1988 (5 vol%, equivalent to ~4.5wt.%) also decomposed this would result in an addition mass loss of ~2.2wt.%. The expected mass loss from both troilite and calcite (2.7wt.%) therefore matches closely with the empirical observations from TGA (2.72wt.%). These data demonstrate a clear absence of phyllosilicates, confirming that Dho 1988 is fully dehydrated.

6. Discussion

6.1. Dho 1988 is a member of the CY group

Dho 1988 has a heavy bulk O-isotope composition (Fig.1, $\delta^{17}O$: 9.2‰, $\delta^{18}O$: 19.5‰ and $\Delta^{18}O$: -1.2‰ [Bouvier et al., 2017b]) and a sulphide-rich mineralogy (14 vol%). These two features are the most prominent primary characteristics of the CY chondrite group. In addition, Dho 1988's average chondrule size (520µm) and low chondrule/CAI abundance (<20 area%) are consistent with the range reported from the literature for other CY members, which have average chondrule sizes of ~420µm and combined chondrule/CAI abundances averaging 18 area%. Thus, although the amount of fine-grained matrix in Dho 1988 (60-70 area%) is similar to that found in CM chondrites (~70 vol%, Weisberg et al., 2006), the average chondrule size in Dho 1988 is distinctly larger than CM average. Furthermore, the parent body alteration history of Dho 1988 (as detailed below) is wholly consistent with the alteration history of all other CY chondrites. We therefore propose that Dho 1988 belongs within the CY group and should be reclassified as such.

6.2. An initial episode of aqueous alteration

6.2.1. Evaluating the extent of pre-metamorphic aqueous alteration in Dho 1988: Although phyllosilicate no longer survives in Dho 1988, evidence for its former existence is clear (section 4.1). All the secondary olivine in Dho 1988 was previously phyllosilicate. By analysing the texture (Figs.2 & 4), composition (Fig.4) and abundance (Table.3) of the secondary olivine in Dho 1988 inferences can be made regarding the state of the parent body after aqueous alteration and before thermal metamorphism.

In hydrated CM chondrites the degree of aqueous alteration can be evaluated in several ways, either by petrographic analysis of polished sections under SEM (notably the Rubin and Browning scales [Browning et al., 1996; Rubin et al., 2007]) or by bulk techniques that analyze larger and more

representative sample volumes (notably the Howard scale [Howard et al., 2009; 2011; 2015]). Here we employ the scheme of Howard et al., (2015) as it is applicable to all carbonaceous chondrites. Based on its bulk modal mineralogy (and accepting that all the secondary olivine was previously phyllosilicate), we calculated a phyllosilicate fraction (given as: total phyllosilicate/total anhydrous silicate + total phyllosilicate [Howard et al., 2015]) for Dho 1988 of 0.85 (Fig.8), which corresponds to a petrologic type 1.3 in the scheme of Howard et al., (2015). Fig.8 shows the inferred phyllosilicate fraction data calculated for other CY chondrites, based on data previously published in King et al., (2015; 2019). They form a sequence from least to most altered: B-7904<Y-86720<Dho 1988<Y-86789<Y-980115=Y-86029=Y-82162 and vary between petrologic grades 1.6 to 1.0. This is similar to the range covered by the CM chondrites.

6.2.2. Phyllosilicate formation: The initial stages of alteration in Dho 1988 were fluid-rich and produced abundant phyllosilicate with Fe-Mg-serpentine compositions (Fig.4B). Relatively high abundances of Ni measured in EDS spot analyses on the sample's groundmass (Fig.4C) combined with the observation of micron/submicron-sized Fe-rich grains (either metal, metal-oxide or sulphides [compositions are uncertain since they are too small to analyse with EDS techniques Fig.3 and 4]) strongly suggest that much of Dho 1988's matrix was composed of fine-grained tochilinite-cronstedtite intergrowths (TCIs). TCIs are one of the main components in the matrix of the hydrated CM chondrites (Rubin et al., 2007; Hewins et al., 2014) and form from several different precursor minerals (for example originating from both the alteration of Fe-Ni metal and amorphous Fe-Mg silicates, Pignatelli et al., 2016). Recent experimental data have constrained the formation of TCIs to low-temperature (<160ºC), weakly alkaline (pH7-8), redox conditions (log fO_2 ~ -54 to -60) (Vacher et al., 2019a). The (inferred) presence of tochilinite therefore provides constraints on the environmental conditions during aqueous alteration in Dho 1988 and by inference the CY group.

Dho 1988 previously contained two main species of phyllosilicate, an Al-rich and an Al-poor species (Fig.4C). The Al-poor species was fine-grained, significantly more abundant and common within the matrix (forming the TCI structures described above). In contrast, the Al-rich species also contained relatively high Na concentrations (~1.8wt.%) and occurred only in the altered chondrule and CAI cores. The (inferred) presence of these two distinct phyllosilicate species have been described in CY chondrites (e.g. B-7904, Tomeoka, 1990 and Y-86720, Tomeoka et al., 1989b). Normalized cation compositions from (former) phyllosilicates in Dho 1988 (Si-Fe-Mg ternary shown in Fig.4B) suggest that the dominant (Al-poor) phyllosilicate species were serpentines, their Mg-rich compositions pointing towards formation in the advanced stages of aqueous alteration (Howard et al., 2009; 2011; Velbel et al., 2012). Conversely, the Al-rich phyllosilicates are more difficult to identify as their compositions fall between the compositional ranges of serpentine and saponite and, due to thermal metamorphism their phyllosilicate crystal lattice structures have been destroyed (e.g. Fig.7 in Akai, 1992, showing disordered phyllosilicates in B-7904). Based on cation chemistry and textures previous studies have suggested these phases are Na-bearing saponite, talc or phlogopites (Tomeoka et al., 1989a; Ikeda, 1991; 1992). Saponite is the most likely phase being relatively common in other hydrated chondrites, notably the CI chondrites (Tomeoka and Buseck, 1988) and the ungrouped C2 chondrites Bells (Brearley, 1995) and Tagish Lake (Zolensky et al., 2002).

Geochemical modelling by Zolotov (2012) explored the formation of several aqueous alteration minerals. They used a CI chondrite starting composition, with isochemical behaviour, water-to-rock ratios (W/R) around 1 and a pressure of 1MPa (above water saturation). Under equilibrium conditions Na-rich saponite can form at temperatures T>130ºC, reaching abundances equal to that of serpentine at T~230ºC. Conversely, Na-rich phlogopite forms at T>110ºC while talc forms at T>160ºC (Zolotov, 2012). Other phases found in CYs and formed by aqueous alteration include chromite (see section 5.2.3), which provides constraints of T<290ºC, and whitlockite (T>100ºC). Finally, the main S-bearing phase formed during aqueous alteration was likely tochilinite which develops at temperatures between 120-160ºC (Vacher et al., 2019a). Collectively the aqueously altered mineral assemblage constrains the alteration environment to a narrow temperature range – the inferred existence of

saponite provides a minimum temperature of 110ºC, while the inferred existence of tochilinite limits temperatures to below 160ºC (Zolotov, 2012; Vacher et al., 2019a). Finally, Na-bearing minerals grow in equilibrium with alkaline NaCl solutions (brines) (Zolotov, 2012). Thus, higher Na contents in precipitated minerals correspond to progressively more concentrated brines. The presence of Na-bearing silicates in CY chondrites requires a saline alteration fluid, although this may have been highly localised in extent and limited to chondrule cores.

6.2.3. Late stage aqueous alteration, Cr-spinel and ilmenite precipitation: Dho 1988 contains micron-scale refractory oxides (Fe-bearing Cr-spinels and Mg-bearing ilmenite grains [Table.2]). These oxides appear as overgrowths on the margins of (former) coarse-grained phyllosilicates and are found only in the altered cores of chondrules and CAIs (Fig.5D and 4E). Their textural relationships require that primary silicates were aqueously altered to form coarse-grained phyllosilicates (of the Al-rich variety) before the refractory oxides grew. Furthermore, the refractory oxides are located only along grain margins, and are not found along the walls of dehydration cracks, rather being cross-cut by them. Thus, the spinel and ilmenite grains formed after phyllosilicate growth but before phyllosilicate dehydration (and later recrystallization into secondary olivine). Consequently, the refractory oxides were derived by precipitation from aqueous fluids.

Tomeoka (1990) also reported the occurrence of Mg-Al-bearing chromites in B-7904. They occur as small refractory spinels forming dense clusters closely associated with (former) phyllosilicates (and located within altered chondrule or CAI cores). This occurrence is therefore identical to the features observed in Dho 1988. Likewise, ilmenite is common as a minor phase in CY chondrites (Y-86720, Tomeoka et al., 1989b; B-7904, Bischoff and Metzler, 1991; Y-86029, Tonui et al., 2002 and the possible CY Dho 735 in Ivanova et al., [2010]). The co-occurrence of both ilmenite and Cr-spinels on the margins of former phyllosilicates demonstrate they formed together, most likely by the aqueous alteration of refractory-rich phases – for example Ti-rich fassaite as observed by Tomeoka and Buseck (1990) in CV chondrites or derived from perovskite alteration, as suggested by Bischoff and Metzler (1991). In Dho 1988, because the refractory oxide phases are only found within the cores of altered chondrules/CAIs, dissolved Ti and Cr ions could not have been transported far from their site of dissolution.

The presence of Cr-spinel and ilmenite co-existing with magnetite (found in some CY chondrites but absent from Dho 1988), phosphates (apatite and whitlockite [Skirius, 1986; Tonui et al., 2002]) and carbonates within the CY lithology suggests that alteration conditions were oxidizing, at least during the later stages when chromite precipitated. In any chondrite where magnetite forms under equilibrium conditions, the redox state of the alteration system must exceed the fugacity of the iron-wüstite buffer. It is therefore possible that environmental conditions evolved considerably during aqueous alteration, transitioning from an initial low-temperature reducing alkaline system required for the formation of TCIs (Vacher et al., 2019) to a fluid-poor oxidizing environment required for the precipitation of Cr-spinel and ilmenite.

6.2.4. The timing of brecciation and its relationship to aqueous alteration: A striking feature of Dho 1988 is the meteorite's brecciated texture and resulting separation into clasts and veins (Fig.2). Dho 1988 is a monomict breccia composed of multiple clasts each derived from same lithology. Although clasts have experienced subtly different degrees of aqueous alteration, as demonstrated by variations in the relative abundance of unaltered primary mafic silicate (appearing as homogenous deep blue regions in Fig.2A), overall, the extent of aqueous alteration across the sample is similar. This contrasts with meteorites, such as the CM chondrite Boriskino (composed of both CM1 and CM2 clasts), that have pronounced differences in alteration extent between their constituent clasts (Verdier-Paoletti et al., 2019). The small and local variations in the degree of aqueous alteration seen in Dho 1988 are common in carbonaceous chondrites and most likely arise due to variations in the primary accretionary rock; variations in the initial porosity or the amount of water accreted during formation (Le Guillou and Brearley, 2014; Jilly-Rehak et al., 2018; Howard and Zanda, 2019).

Based on the presence of aqueous alteration products (phyllosilicates, sulphides and carbonates) that infill the fractures formed by brecciation we can infer that the aqueous alteration was active after fracturing. By contrast, whether aqueous alteration was active prior to brecciation remains unclear. We find no unambiguous textural evidence (for example, the presence of phyllosilicate phases that have been cut by the fractures) to support pre-brecciation aqueous activity.

6.2.5. The formation of carbonates: As a broad generalisation the clasts in Dho 1988 are composed primarily of silicates, while the veins contain a close association of sulphides and carbonates. However, careful observation of the veins in Dho 1988 shows that they are zoned with two main layers (Fig.2A, 4A, Fig.S2). The outer regions have a dark highly porous appearance. This layer contains Al, Si, Mg, Fe and S and is therefore most likely a mix of Fe-sulphides and (the thermal decomposition products of former) phyllosilicates. Conversely, the vein's core is composed of carbonate masses containing embedded sulphides (troilite) with irregular shapes and sub-rounded textures. The presence of (former) phyllosilicate within the veins requires that the fractures formed by brecciation served as pathways for circulating fluids. Since veins form by precipitation of minerals from fluids, vein growth occurs from the wall inwards, allowing the sequence of mineralisation to be reconstructed. In Dho 1988 a combined growth of phyllosilicates and (minor) sulphides precipitated first. Later, the carbonate-sulphide core formed. However, because sulphide grains are always enclosed within carbonate hosts, the law of included fragments requires that the carbonate mineralogy formed after the sulphides.

Previous studies on other CY chondrites have also reported carbonate veins. Tomeoka (1990 [Fig.21]) identified abundant thin (<2µm) Ca-carbonate vein networks within the matrix of B-7094 (an Antarctic find) similar to the small veins seen in Dho 1988 (Fig.5B), while Ivanova et al., (2010) reported Ca-carbonate veins in the probable CY chondrite Dho 735 (a hot desert find), although no BSE images were shown so their morphology is unknown. Carbonates in Dho 1988 and other CY chondrites may originate either as a parent body mineralisation event or represent recent terrestrial weathering.

Endogenous carbonates are relatively common in carbonaceous chondrites and occur as large euhedral monomineralic grains, polymineralic grain clusters or as veins infilling fractures (Lee et al., 2012; 2013; 2014). In the CM chondrites several species of carbonate are known, including breunnerite, calcite and dolomite. Multiple analyses of carbonates in other CM chondrites have concluded that alteration occurred on a prograde path (becoming progressively hotter) and that calcite formation occurred in two distinct episodes (de Leuw et al., 2010; Lee et al., 2012; 2013; 2014; Lindgren et al., 2017; Vacher et al., 2019b). Early generation calcite grains (termed T1) were formed at low-temperatures (10-100ºC, Vacher et al., 2019b) prior to the main growth windows for phyllosilicate and sulphides. These early calcites may have co-precipitated with (or precipitated shortly before/after) other complex carbonates (e.g. breunnerite) facilitated by the presence of Mg-rich solutions. Meanwhile the later generation of calcites (termed T2) formed at higher temperatures of 110-245ºC (Vacher et al., 2019b) after the growth of phyllosilicate and sulphides. The second generation (T2) calcites replaced primary ferromagnesian silicates as well as infilling fractures to form veins (Lee et al., 2013). Thus, in CM chondrites T2 calcites may contain Fe-sulphide inclusions, while the T1 calcites instead have overgrowth mantles of sulphides and/or phyllosilicates. If carbonate mineralization in the CY chondrites followed a similar evolution to that of the CM chondrites, then the calcite in Dho 1988 appears "*T2-like*" and may have formed during late-stage aqueous alteration. Both the vein calcite and the carbonate chondrule pseudomorph (Fig.3F) contain Fe-sulphide inclusions, while the chondrule pseudomorph attests to the replacement of silicate phases by carbonate.

Alternatively, carbonate can form by terrestrial weathering in both hot desert and Antarctic meteorites. For example, Tyra et al., (2007) argued that veins of hydrated Mg-rich carbonate (hydromagnesite) within Antarctic CM chondrites formed as a result of silicate weathering reactions. Isotopic evidence suggests they can use either atmospheric or meteorite-derived carbon, complicating the identification of terrestrially formed carbonate veins (Tyra et al., 2007). Importantly, weathering-derived carbonate veins and infill features (Tyra et al., 2007, Fig.3E, 2G and 2H) contain embedded

hydrated S-bearing minerals (commonly sulphate) and their textures can appear similar to those observed here in Dho 1988. Abreu and Brearley (2005) reported carbonate veins (<25µm) extending for several 100µm and cross-cutting the fusion crust in the CV chondrite Vigarano. In the same sample they also observed carbonate pseudomorphs after augite crystals within a porphyritic chondrule. Abreu and Brearley (2005) concluded that the calcite pseudomorphs were parent body in origin while all other carbonate morphologies (namely the veining) were terrestrial.

With the current data it is not possible to conclusively constrain the origin of carbonates in Dho 1988. However, a pre-terrestrial (parent body) origin seems likely. This interpretation is based on several factors: (1) Carbonate veins in Dho 1988 contain reduced sulphides (troilite) rather than oxidized sulphate minerals which are otherwise typical in weathering-derived carbonate veins (Lee and Bland, 2004). Thus, if the carbonate veins were present when the meteorite fell, they could have protected the sulphides from oxidation. (2) There appears to have been a single episode of carbonate formation, as evidenced by their similar chemical compositions (despite different morphologies) and this carbonate growth likely occurred either shortly after sulphide formation, in order to produce the enclosed sulphide grains seen in the large mineralized veins. (3) The pseudomorphic carbonate chondrule in Dho 1988 (Fig.2A and 2F) appears similar to other carbonate chondrule pseudomorphs described by Lee et al., (2014 [Fig.22B & 12C]) within the CM chondrite Pollen. Lee et al. (2014) interpreted these as second-generation calcites, formed on the parent body. (4) Finally, near-identical carbonate-sulphide veins can be found in Y-82162 (as we demonstrate in Fig.S4). They have embedded irregular-shaped troilite masses held within a Ca-carbonate host and have a similar zoned texture with darker margins nearly-identical to those found in Dho 1988. However, the carbonate-sulphide veins in Y-82162 have considerably less sulphide and occur much less frequently, although this may reflect differences in their parent body alteration histories. Because similar vein features are found in both hot desert and Antarctic CY chondrites this adds weight to the hypothesis that the carbonate-sulphide veins predate terrestrial alteration and are therefore parent body in origin.

6.3. Thermal metamorphism

6.3.1. Peak metamorphic temperature estimates: Thermal metamorphism occurring after aqueous alteration is relatively common in carbonaceous chondrites and affects ~36% of the 39 CM/C2ung meteorites studied by Quirico et al. (2018).

Broad constraints on the peak metamorphic temperature can be derived from the behaviour of phyllosilicate dehydration, dehydroxylation and recrystallization. At low pressure, serpentine minerals begin to dehydrate at T>300ºC, form highly disordered dehydroxylates between 400-500ºC and develop into poorly-crystalline olivine at T>500ºC (Akai, 1992; Nakamura, 2005; Nozaki et al., 2006; Nakato et al., 2008). As temperatures rise further, olivine crystallinity matures. In contrast to serpentine, saponite is more heat-resistant and decomposes to an amorphous phase around 700ºC before transforming to enstatite at T>850ºC (Akai, 1992; Che et al., 2011; Che and Glotch, 2012). Data derived from XRD measurements in King et al., (2015; 2019) show that dehydroxylated amorphous material without coherent diffraction peaks is detectable in Y-82162, Y-86029 and Y-98015, whereas the remaining CYs (Y-86720, Y-86789 and B-7904) contain no discernible dehydroxylates and instead their phyllosilicates have been completely recrystallized, forming secondary olivine and possibly also a minor quantity of pyroxene (<11 vol%). This demonstrates that individual CY chondrites experienced either different peak temperatures and/or different durations of heating.

Nakamura (2005) proposed a classification system for thermally metamorphosed hydrated carbonaceous chondrites based on the behaviour of phyllosilicate decomposition and recrystallization as measured by XRD. This system provides grades ranging from stage I to IV, corresponding to unheated chondrites that produce coherent phyllosilicate diffraction peaks (stage I, <300ºC), moderately heated samples in which phyllosilicates are highly disordered (stage II, 300-500ºC), advanced metamorphism in which poorly recrystallized, econdary olivine produces weak diffraction peaks (stage III, 500-750ºC) and intensely heated samples with an anhydrous mineralogy and well-

developed recrystallized olivine peaks (stage IV, >750ºC). Nakamura (2005) classified Y-82162 and Y-86029 with heating stage III (500-750ºC), whereas Y-86720, Y-86789 and B-7904 were designated as having characteristics of heating stage IV (>750ºC).

Alternative methods also provide estimates of peak metamorphic temperature. Nakato et al., (2008) studied Mg-Fe diffusion profiles in primary olivine from B-7904 and concluded that heating was short-lived allowing unequilibrated mineral assemblages to survive. They suggested either 10-10^3 days at 700ºC or 1-100 hours at 890ºC. Later, Kikuchi et al., (2015) studied Y-980115 and concluded that heating either lasted for ~100 minutes at temperatures >500ºC or that heating was longer duration (unspecified how long) and within the range of 500-600ºC. This estimate was based on both the co-existence of carbonate and carbonate decomposition products (periclase) and the relatively low noble gas budget of the sample. Additionally, Kimura et al., (2011) identified micron-sized schreibersite grains within Fe-Ni metal in B-7904 and suggested that their partitioning behavior requires metamorphic temperatures around 920ºC.

In Dho 1988 neither serpentine nor saponite survive, and the matrix has largely recrystallized into a metamorphic groundmass of secondary olivine. Dho 1988 therefore reached at least heating stage III (500-750ºC) in the system of Nakamura (2005). The decomposition of the coarse-grained phyllosilicates (which are most likely saponite [section 5.2.2]) suggests a minimum peak metamorphic temperature of >700ºC. In addition, Dho 1988 also contains calcite, primarily within veins but also replacing a single chondrule (Fig.3F). Assuming this calcite is parent body in origin, (as opposed to a terrestrial weathering product [section 5.2.3.]) its decomposition behaviour potentially provides further constraints on the peak metamorphic temperature.

Calcite thermally decomposes to Ca-oxide in a decarbonation reaction. Thermo-gravimetric analysis provides information on the thermal decomposition behaviour of phases at low pressures, relevant to asteroids. Our calcite standard (NHM collection ID: BM 44296, Fig.S3) began to decompose at temperatures above 600ºC. Initially the rate of decomposition is slow but increases rapidly above 750ºC, peaking at ~770ºC. Independent studies show near identical behaviour with decomposition above 675ºC, and peak release around 790ºC (Ptáček et al., 2017; Kohobhange et al., 2019). Although decomposition behaviour is also dependent on the cation composition, grain size and crystallinity of calcite as well as (in TGA experiments) analytic factors such as the purge gas composition, flowrate and sample weight (Salvador et al., 1989; Valverde et al., 2015), they have relatively minor effects on decomposition temperature, resulting in changes of <100ºC (Salvador et al., 1989; Valverde et al., 2015). In Dho 1988 the absence of crystalline Na-saponite and the retention of (at least some crystalline) calcite provides temperature constraints on the peak metamorphic temperature experienced by Dho 1988: 700ºC<PMT<800ºC.

6.3.2. Troilite grains and sulphur mobilisation: Prior to thermal metamorphism, sulphur was likely held within tochilinite and/or pyrrhotite with minor quantities found in organic compounds. Tochilinite is common in the less altered CM2 chondrites (Browning and Bourcier, 1996; Howard et al., 2011; Vacher et al., 2019). In more intensely altered chondrites, including some CM2s, the CM1s and the CIs, the most common S-bearing mineral is pyrrhotite, which co-occurs with minor pentlandite (Bullock et al., 2005; Howard et al., 2011; King et al., 2015a; 2017). Finally, in hydrated and then thermally metamorphosed carbonaceous chondrites (e.g. some CMs and the CY class), troilite is the most common S-host (Harries and Langenhorst, 2013).

The pre-metamorphic mineral assemblage in Dho 1988 likely contained both TCIs (as argued in section 5.2.2.) and well-developed pyrrhotite masses. Pyrrhotite would have been more common than tochilinite, as evidenced by the presence of many large S-bearing grains not intimately mixed with phyllosilicate. These two minerals were later converted to troilite during metamorphism.

Previously, Harries and Langenhorst (2013) investigated the behaviour of S-bearing minerals in two CY chondrites (B-7904 and Y-86720) using transmission electron microscopy (TEM) to explore the relationships between sulphides, metal and oxides. They found that both CYs are dominated by troilite

but also contain small quantities of metal. Harries and Langenhorst (2013) demonstrated that pyrrhotite thermally decomposes along two different pathways, producing either Fe-metal or troilite and in both reactions sulphur gas is liberated. Given that troilite compositions in Dho 1988 and all other CY chondrites are stoichiometrically ideal (e.g. Bischoff and Metzler, 1991), sulphide fugacities (fS_2) on the CY parent body must have been low, in equilibrium with metal, and thus held at the iron-troilite buffer.

Magnetite is absent in Dho 1988; however, this mineral does occur in some CY chondrites, notably in Y-82162, Y-86029 and B-7904 (Tomeoka et al., 1989a; Bischoff and Metzler, 1991; Zolensky et al., 1993). Magnetite would have formed during aqueous alteration but its presence in some CY meteorites requires survival of this phase through later thermal metamorphism. Harries and Langenhorst (2013) suggested that iron, magnetite and pyrrhotite can coexist in equilibrium. However, their discussion of the Fe-S-O system ignored the effects of Ni. Since the Ni-NiO buffer sits well above the FeO-Fe_3O_4 buffer (whereas Fe-FeO sits well below FeO-Fe_3O_4, as shown in Fig.9), the presence of Ni has the effect of stabilising Fe metal. This is important because it allows the redox system to persist on the FeNi-FeS buffer at high temperatures in a relatively oxidised system, whilst responding through the continual release of S_2 gas with increasing temperature.

In a variety of petrographic settings, magnetite is found to coexist with Ni-rich metal, commonly awaruite (Filippidis 1985). Magnetite-awaruite assemblages occur in CVoxA chondrites where they are associated with hydrothermal alteration (Bonal et al., 2020) and were previously reported in Y-82162 by Zolensky et al., (1993) and in Y-86029 by Tonui et al., (2002). If one followed the arguments of Harries and Langenhorst (2013), the CY mineral assemblage would imply that the magnetite-bearing meteorites were heated to T<572ºC, whereas magnetite-free CY chondrites were heated above this temperature. However, this interpretation is contrary to most other peak metamorphic temperature estimates, such as those based on phyllosilicate decomposition (Akai, 1992; Nakamura 2005) and is therefore likely incorrect. A clear example of why magnetite-bearing CYs must have been heated to higher temperatures than the 572ºC can be found in the magnetite-bearing B-7904. This meteorite experienced the highest peak temperatures of the all the CY meteorites (>750ºC) as evidenced by the decomposition of saponite (Nakamura, 2005), well-crystallized secondary olivine (King et al., 2019) very low water contents (<2.6 wt.%, Haramura et al., 1983) and the presence of plessitic textured metal grains, formed by high-temperature alteration (Kimura et al., 2011).

The sulphide-metal-oxide mineral assemblage in Dho 1988 is most similar to that documented for Y-86720 (Harries and Langenhorst 2013). Dho 1988 is dominated by stoichiometrically pure troilite grains and contains minor metal (Fig.5H & 4I), while Fe-oxides are absent. Metal occurs in close association with troilite either as dispersed micron-size rounded grains within the matrix or as irregular-shaped regions held within or in direct contact with troilite masses. Troilite grains in Dho 1988 are generally large (>50µm) rounded grains (as in Fig.5C), but smaller irregular-shaped masses with variable but relatively high porosities are also common (as in Fig.5H); thus, two generations of troilite may exist.

Some of the larger troilite grains in Dho 1988 most likely formed by the devolatilization of pyrrhotite during thermal metamorphism at temperatures 400ºC<T<600ºC (Fig.S5). However, peak metamorphic temperatures in Dho 1988 would have continued to rise, leading the system's oxygen fugacity to intersect the troilite-iron buffer and resulting in a small amount of thermal decomposition from troilite, forming metal at temperatures T>º635C (Fig.7). This would have liberated S_2 gas, which could then travel through the rock, tending to preferentially consume any magnetite that was likely present (and previously produced by aqueous alteration). Sulphur gas could potentially also scavenge Fe from silicates (Tomkins, 2009). However, because fS_2 was held at the FeNi-troilite buffer, sulphur gas would also recombine with FeNi-metal to form troilite during cooling, and also with troilite isolated from metal to form the pyrrhotite rims – as suggested by Harries and Langenhorst (2013). Both mechanisms would form a second generation of sulphide grains. Thus, sulphur mobilization explains the existence of troilite grains within features such as phyllosilicate dehydration cracks that formed

during metamorphism. The absence of magnetite in Dho 1988 (Fig.5H and 4I) allowed fS_2 to reach the FeNi-troilite buffer at lower fO_2 during progressive heating.

6.4. Summarizing the alteration history of Dho 1988

Dho 1988 was heavily affected by both aqueous alteration and thermal metamorphism. However, impact brecciation also played a significant role in this meteorite's history. Whether impact heating initiated aqueous alteration or whether impacts occurred during aqueous alteration remains unclear. In either case, aqueous alteration later evolved into thermal metamorphism as water-to-rock ratios decreased and temperatures rose (Fig.10).

The early stages of aqueous alteration in the CY chondrites appear to have been most similar to those of the CM chondrites. High W/R ratios paired with low-to-moderate temperature (110ºC<T<160ºC) alteration under reducing conditions led to hydration of the matrix. Initially, this resulted in the formation of widespread TCIs. However, as alteration advanced, pyrrhotite replaced tochilinite as the dominant S-bearing mineral and magnetite precipitated from solution. Meanwhile anhydrous chondrule silicates were progressively replaced by phyllosilicate. The degree of aqueous alteration was variable across the parent body allowing the preservation of some nearly unaltered chondrules co-existing with other entirely pseudomorphic forms. During the advanced stages of aqueous alteration refractory phases present in chondrules and CAIs were dissolved and rapidly precipitated forming Cr-spinel and Mg-ilmenite overgrowths on coarse-grained phyllosilicates.

Open fractures (formed by impact) were exploited by fluids and progressively mineralized. Initially a mixed assemblage of sulphides and phyllosilicates were deposited along fracture walls. By contrast, the late-stage inner regions of veins are composed of mixed calcite and sulphide. Here, calcite encloses sulphides suggesting calcite was the last phase to form. The presence of carbonate both between clasts and within clasts, as well as the occurrence of a single chondrule pseudomorph composed of carbonate (all with similar chemical compositions) combined with the presence of sulphide (as opposed to sulphate) suggest that carbonate formation was a parent body process and not a terrestrial weathering feature.

Later, Dho 1988 was affected by a significant episode of thermal metamorphism. If the brecciation in this meteorite was caused by a high-energy impact event, the post brecciation aqueous alteration that formed vein phyllosilicates may have then evolved directly into a metamorphic event as post-shock temperatures rose. At temperatures between 400-600ºC pyrrhotite thermally decomposed to form troilite and Fe-metal as well as liberated S_2 gases. Meanwhile serpentine decomposed to highly disordered dehydroxylates before recrystallizing as secondary olivine. At higher temperatures, saponite dehydrated and may have partially recrystallized to form small quantities of pyroxene. Significant volume contraction in phyllosilicates led to the development of an extensive dehydration crack network. During the retrograde metamorphic cooling, the liberated S_2 gas (from decomposed sulphides [mainly pyrrhotite]) facilitated a brief episode of sulphidization. However, S_2 gas did not travel far within the meteorite before reacting with Fe and forming a second generation of troilites. This reaction explains the absence of Fe-oxides (magnetite), the low-Ni troilite compositions and the mobilization of sulphur into dehydration cracks. The presence of stoichiometrically pure troilite, co-existing with minor quantities of Fe-metal (in all of the CYs) constrains fS_2 to the iron-troilite buffer in these chondrites.

7. Implications

7.1. Geographic locations of recovered CY chondrites: Over time new carbonaceous chondrite groups have been recognized, as several meteorites with closely related properties have been discovered and described (Weisberg et al., 2006). To define a new group requires the presence of at least five unpaired meteorites (Weisberg et al., 2006). Currently there are six Antarctic CY chondrites, all recovered from the Yamato mountains in East Antarctica (King et al., 2019). Among these Y-86720 and Y-86789 are described as paired by Matsuoka et al. (1996).

This study demonstrates that Dho 1988 should be included in the CY chondrite group, and thus that CY meteorites can be found outside Antarctica. Likewise, the previous work of Ivanova et al., (2010) concluded that Dho 735 and Dho 235 have similar primary characteristics and alteration histories to Y-86029 and B-7904 – strongly suggesting they are also CY chondrites. As indicated in section 2, there are several other potential CY members among the Dhofar meteorite population based upon their descriptions in the Meteoritical Bulletin (Dho 955 [Russell et al., 2005; Ivanova et al., 2005]) and notably on their bulk O-isotope compositions (Dho 2046 [Bouvier et al., 2017a] and Dho 2066 [Gattacceca et al., 2019]). However, it should also be noted that several of the Dhofar samples (Dho 735, Dho 955 and Dho 2066) could be paired (Table.1), having been found within 3km of each other.

The landscapes of both geographic locations where CY chondrites have been recovered are young. The inferred terrestrial residence times of Yamato mountains meteorites lie between 35,000-70,000 years (Zolenky et al., 2005), while carbon-14 age dating of 50 ordinary chondrites from Dhofar revealed ages between 2,000-49,000 years, with a median age of 17,900 years (Al-Kathiri et al., 2005). The absence of CY chondrites from older terrestrial sites implies that they are fragile, highly susceptible to terrestrial weathering and unlikely to survive for >100,000 years exposed at the Earth's surface.

Interestingly however, no CY members have yet been identified among the Northwest Africa (NWA) site, which has a similarly young terrestrial age (~4,000 to 40,000 years, Aboulahris et al., 2019) to the Dhofar and Yamato regions. The lack of CYs from NWA could be due to the infancy of this meteorite group combined with the lack of widespread adoption of the CY designation by the community after their initial proposal (Ikeda, 1992). However, with renewed research on these meteorites (King et al., 2019) and additional members now identified in Oman we anticipate that future studies will identify CY chondrites from the NWA location and potentially other meteorite fields with young terrestrial ages.

7.2. Problems of classification: The distinctive alteration history of the CY chondrites (and other hydrated and subsequently dehydrated carbonaceous chondrites [~1/3 of the 39 CM/C2ung meteorites studied by Quirico et al. (2018)]) present problems for sample characterisation and challenge the established classification nomenclature. For example, in this study Dho 1988 no longer contains phyllosilicate so classification as a type II specimen (a CY2 in the system of van Schmus and Wood [1967]) would be incorrect. However, classification as a type III meteorite is likewise misleading (contrary to the suggestion of Ebert et al., [2019] who argued that the hydrated-then-dehydrated CM chondrite NWA 11024 should be considered a CM3). Instead we support the suggestion of Tonui et al., (2014) which argues that carbonaceous chondrites are best described by a revised two part system combining van Schmus and Wood (1967) with Nakamura (2005). This would classify Dho 1988 as a CY2, stage IV sample.

8. Conclusions

Dho 1988 should be reclassified as a CY2 chondrite, with a stage IV thermal history (in the scheme of Nakamura [2005]). Dho 1988 and the other CY chondrites are united by heavy oxygen isotope compositions (approximately: $\delta^{17}O$: 10.8‰, $\delta^{18}O$: 21.5‰ and $\Delta^{18}O$: -0.3‰), high sulphide abundances (>15 vol% occurring primarily as stoichiometrically ideal troilite) and medium-sized chondrules (typically >400µm). They also share a common alteration history defined by aqueous alteration overprinted by thermal metamorphism. This has produced their characteristic dehydrated mineralogies, low water abundances and low volatile trace element abundances. The CYs have an exotic array of accessory minerals including (former Na-bearing saponite) Cr-spinel, ilmenite, phosphates and (in some members) periclase.

We used cross-cutting relationships to reconstruct the complex geological history of Dho 1988's parent body. Accretionary phases and textures were progressively replaced by hydrated phases (TCIs, serpentine, Na-saponite, refractory oxides and pyrrhotite). Brecciation produced fractures that

increased porosity and permeability resulting in the formation of mineralized veins. Finally, thermal metamorphism led to the dehydration of phyllosilicates and their subsequent recrystallisation of secondary olivine, as well as the decomposition of sulphides and the partial decomposition of carbonates. On cooling, mobilized sulphur gas reacted (with magnetite) to form a new generation of troilite, infilling voids generated by dehydration.

CY chondrite meteorites are currently known only from the Yamato Mountains Antarctic site and the Dhofar region of Oman. Both sites have relatively young terrestrial ages, suggesting that CY chondrites do not withstand terrestrial weathering. We expect additional CY chondrite meteorites to be identified among other meteorite collect sites with similarly young terrestrial ages (<75,000 years), notably from the NWA location.

9. Acknowledgements

This research was funded by the Science and Technology Facilities Council (STFC), UK, through the grant ST/R000727/1 – *The geological history of water-rich asteroids*. We thank Museum für Naturkunde Berlin for the loan of the subject meteorite Dhofar 1988. We are also grateful to Jérôme Gattacceca and an anonymous reviewer for their insightful comments as well as to Eric Quirico for the handling of this manuscript.

10. References

1. Aboulahris, M., Chennaoui Aoudjehane, H., Rochette, P., Gattacceca, J., Jull, A.T., Laridhi Ouazaa, N., Folco, L. and Buhl, S., (2019). Characteristics of the Sahara as a meteorite recovery surface. *Meteorit. Planet. Sci.* **54**, 2908-2928, doi:10.1111/maps.13398.
2. Akai, J., (1990). Mineralogical evidence of heating events in Antarctic carbonaceous chondrites Y-86720 and Y-82162. *Antarc. Met. Res.* **3**, 55-68.
3. Akai, J., (1992). T-T-T Diagram of Serpentine and Saponite, And Estimation of Metamorphic Heating Degree of Antarctic Carbonaceous Chondrites. *Antarc. Met. Res.* **5**, 120-135.
4. Alexander, C., M., O'D., Greenwood, R.C., Bowden, R., Gibson, J.M., Howard, K.T. and Franchi, I.A., (2018). A mutli-technique search for the most primitive CO chondrites. *Geochim. Cosmochim. Acta* **221**, 406-420, doi:10.1016/j.gca.2017.04.021.
5. Al-Kathiri, A., Hofmann, B.A., Jull, A.T. and Gnos, E., (2005). Weathering of meteorites from Oman: Correlation of chemical and mineralogical weathering proxies with 14C terrestrial ages and the influence of soil chemistry. *Meteorit. Planet. Sci.* **40**, 1215-1239, doi:10.1111/j.1945-5100.2005.tb00185.x.
6. Bischoff, A., (1998). Aqueous alteration of carbonaceous chondrites: Evidence for preaccretionary alteration—A review. *Meteorit. Planet. Sci.* **33**:1113-1122.
7. Bischoff, A. and Metzler, K., (1991). Mineralogy and Petrology of the Anomalous Carbonaceous Chondrites, Yamato-86720, Yamato-82162, and Belgica-7904. *Antarc. Met. Res.* **4**, 226-246.
8. Bonal, L., Gattacceca, J., Garenne, A., Eschrig, J., Rochette, P. and Ruggiu, L.K., (2020). Water and heat: New constraints on the evolution of the CV chondrite parent body. *Geochim. Cosmochim. Acta,* doi:10.1016/j.gca.2020.03.009.
9. Bouvier, A., Gattacceca, J., Grossman, J. and Metzler, K., (2017a). The meteoritical bulletin, No. 105. *Meteorit. Planet. Sci.* **52**, 2411-2411, doi:10.1111/maps.12944.
10. Bouvier, A., Gattacceca, J., Agee, C., Grossman, J. and Metzler, K., (2017b). The meteoritical bulletin, no. 104. *Meteorit. Planet. Sci.* **52**, 2284-2284, doi:10.1111/maps.12930.
11. Braukmüller, N., Wombacher, F., Hezel, D.C., Escoube, R. and Münker, C., (2018). The chemical composition of carbonaceous chondrites: Implications for volatile element depletion, complementarity and alteration. *Geochim. Cosmochim. Acta* **239**, 17-48, doi:10.1016/j.gca.2018.07.023.
12. Brearley, A.J., (1995). Aqueous alteration and brecciation in Bells, an unusual, saponite-bearing, CM chondrite. *Geochim. Cosmochim. Acta* **59**, 2291-2317, doi:10.1016/0016-7037(95)00107-B.
13. Browning, L.B. and Bourcier, W.L., (1996). Tochilinite: a sensitive indicator of alteration conditions on the CM asteroidal parent body. *Lunar and Planetary Science Conference* (Vol. 27, Abstr#1091).

14. Browning, L.B., McSween Jr, H.Y. and Zolensky, M.E., (1996). Correlated alteration effects in CM carbonaceous chondrites. *Geochim. Cosmochim. Acta* **60**, 2621-2633, doi:10.1016/0016-7037(96)00121-4.
15. Bullock, E.S., Gounelle, M., Lauretta, D.S., Grady, M.M. and Russell, S.S., (2005). Mineralogy and texture of Fe-Ni sulfides in CI1 chondrites: Clues to the extent of aqueous alteration on the CI1 parent body. *Geochim. Cosmochim. Acta* **69**, 2687-2700, doi:10.1016/j.gca.2005.01.003.
16. Burgess, R., Wright, I.P. and Pillinger, C.T., (1991). Determination of sulphur-bearing components in C1 and C2 carbonaceous chondrites by stepped combustion. *Meteoritics* **26**, 55-64, doi:10.1111/j.1945-5100.1991.tb01015.x.
17. Che, C., Glotch, T.D., Bish, D.L., Michalski, J.R. and Xu, W., (2011). Spectroscopic study of the dehydration and/or dehydroxylation of phyllosilicate and zeolite minerals. *J. Geophy. Res. Planet.* **116**, doi:10.1029/2010JE003740.
18. Che, C. and Glotch, T.D., (2012). The effect of high temperatures on the mid-to-far-infrared emission and near-infrared reflectance spectra of phyllosilicates and natural zeolites: Implications for Martian exploration. *Icarus* **218**, 585-601, doi:10.1016/j.icarus.2012.01.005.
19. Choe, W.H., Huber, H., Rubin, A.E., Kallemeyn, G.W. and Wasson, J.T., (2010). Compositions and taxonomy of 15 unusual carbonaceous chondrites. *Meteorit. Planet. Sci.* **45**, 531-554, doi: 10.1111/j.1945-5100.2010.01039.x.
20. Clayton, R.N. and Mayeda, T.K., (1999). Oxygen isotope studies of carbonaceous chondrites. *Geochim. Cosmochim. Acta* **63**, 2089-2104, doi:10.1016/S0016-7037(99)00090-3.
21. de Leuw, S., Rubin, A.E. and Wasson, J.T., (2010). Carbonates in CM chondrites: Complex formational histories and comparison to carbonates in CI chondrites. *Meteorit. Planet. Sci.* **45**, 513-530, doi:10.1111/j.1945-5100.2010.01037.x.
22. Ebert, S., Bischoff, A., Harries, D., Lentfort, S., Barrat, J.A., Pack, A., Gattacceca, J., Visser, R., Schmid-Beurmann, P. and Kimpel, S., (2019). Northwest Africa 11024—A heated and dehydrated unique carbonaceous (CM) chondrite. *Meteorit. Planet. Sci.* **54**, 328-356, doi:10.1111/maps.13212.
23. Ebel, D.S., Brunner, C., Konrad, K., Leftwich, K., Erb, I., Lu, M., Rodriguez, H., Crapster-Pregont, E.J., Friedrich, J.M. and Weisberg, M.K., (2016). Abundance, major element composition and size of components and matrix in CV, CO and Acfer 094 chondrites. *Geochim. Cosmochim. Acta* **172**, 322-356, doi:10.1016/j.gca.2015.10.007.
24. Eggleton, R.A., (1986). The relations between crystal structure and silicate weathering rate. Rates of chemical weathering of rocks and minerals, In Rates of chemical weathering (eds. S. M. Colman and D. P. Dethier) *Academic Press Incorporated*. pp.21-40.
25. Filippidis, A., (1985). Formation of awaruite in the system Ni-Fe-Mg-Si-OHS and olivine hydration with NaOH solution, an experimental study. Econ. Geol. **80**, 1974-1980, doi:10.2113/gsecongeo.80.7.1974
26. Fuchs, L.H., Olsen, E. and Jensen, K.J., (1973). Mineralogy, mineral-chemistry, and composition of the Murchison (C2) meteorite. Smithson. contrib. earth sci. doi:10.5479/si.00810274.10.1
27. Garenne, A., Beck, P., Montes-Hernandez, G., Chiriac, R., Toche, F., Quirico, E., Bonal, L. and Schmitt, B., (2014). The abundance and stability of "water" in type 1 and 2 carbonaceous chondrites (CI, CM and CR). *Geochim. Cosmochim. Acta* **137**, 93-112, doi:10.1016/j.gca.2014.03.034.
28. Gattacceca, J., Bouvier, A., Grossman, J., Metzler, K. and Uehara, M., (2019). The meteoritical bulletin, No. 106. *Meteorit. Planet. Sci.* **54,** 469-471, doi:10.1111/maps.13215.
29. Gattacceca, J., Bonal, L., Sonzogni, C. and Longerey, J., (2020). CV chondrites: More than one parent body. *Earth Planet. Sci. Lett.* **547**, p.116467, doi:10.1016/j.epsl.2020.116467.
30. Greenwood, R.C., Howard, K.T., King, A.J., Lee, M.R., Burbine, T.H., Franchi, I.A., Anand, M., Findlay, R. and Gibson, M., (2019). Oxygen Isotope Evidence for Multiple CM Parent Bodies: What Will We Learn from the Hayabusa2 and OSIRIS-REx Sample Return Missions?. *In 50th Lunar and Planetary Science Conference* (LPI contribution No. 2132), (Abstr.#3191).
31. Greenwood, R.C., Burbine, T.H. and Franchi, I.A., (2020). Linking asteroids and meteorites to the primordial planetesimal population. Geochimica et Cosmochimica Acta, doi:10.1016/j.gca.2020.02.004.
32. Gregory, T., Luu, T.H., Coath, C.D., Russell, S.S. and Elliott, T., 2020. Primordial formation of major silicates in a protoplanetary disc with homogeneous 26Al/27Al. *Sci. Adv.* **6**, p.eaay9626, doi:10.1126/sciadv.aay9626.

33. Greshake, A., Kloeck, W., Arndt, P., Maetz, M., Flynn, G.J., Bajt, S. and Bischoff, A., (1998). Heating experiments simulating atmospheric entry heating of micrometeorites: Clues to their parent body sources. *Meteorit. Planet. Sci.* **33**, 267-290, doi:10.1111/j.1945-5100.1998.tb01632.x.
34. Gooding, J.L. and Zolensky, M.E., (1987). Thermal stability of tochilinite. *In Lunar and Planetary Science Conference* (Vol. 18).
35. Gudbrandsson, S., Wolff-Boenisch, D., Gislason, S.R. and Oelkers, E.H., (2011). An experimental study of crystalline basalt dissolution from 2⩽ pH⩽ 11 and temperatures from 5 to 75° C. *Geochim. Cosmochim. Acta* **75**, 5496-5509, doi:10.1016/j.gca.2011.06.035.
36. Guo, W. and Eiler, J.M., (2007). Temperatures of aqueous alteration and evidence for methane generation on the parent bodies of the CM chondrites. *Geochim. Cosmochim. Acta* **71**, 5565-5575, doi:10.1016/j.gca.2007.07.029.
37. Haramura, H., Kushiro, I. and Yanai, K., (1983). Chemical compositions of Antarctic meteorites I. Memoirs of National Institute of Polar Research. Special issue, **30**, 109-121.
38. Harries, D. and Langenhorst, F., (2013). The nanoscale mineralogy of Fe, Ni sulfides in pristine and metamorphosed CM and CM/CI-like chondrites: Tapping a petrogenetic record. *Meteorit. Planet. Sci.* **48**, 879-903, doi:10.1111/maps.12089
39. Hewins, R.H., Bourot-Denise, M., Zanda, B., Leroux, H., Barrat, J.A., Humayun, M., Göpel, C., Greenwood, R.C., Franchi, I.A., Pont, S. and Lorand, J.P., (2014). The Paris meteorite, the least altered CM chondrite so far. *Geochim. Cosmochim. Acta* **124**, 190-222, doi:10.1016/j.gca.2013.09.014.
40. Howard, K.T. and Zanda, B., (2019). Why is the Degree of Aqueous Alteration Variable? In 82nd Annual Meeting of The Meteoritical Society (Vol. 2157, Abstr.#6178).
41. Howard, K.T., Benedix, G.K., Bland, P.A. and Cressey, G., (2009). Modal mineralogy of CM2 chondrites by X-ray diffraction (PSD-XRD). Part 1: Total phyllosilicate abundance and the degree of aqueous alteration. *Geochim. Cosmochim. Acta* **73**, 4576-4589, doi:10.1016/j.gca.2009.04.038.
42. Howard, K.T., Benedix, G.K., Bland, P.A. and Cressey, G., (2011). Modal mineralogy of CM chondrites by X-ray diffraction (PSD-XRD): Part 2. Degree, nature and settings of aqueous alteration. *Geochim. Cosmochim. Acta* **75**, 2735-2751, doi:10.1016/j.gca.2011.02.021.
43. Howard, K.T., Alexander, C.O.D., Schrader, D.L. and Dyl, K.A., (2015). Classification of hydrous meteorites (CR, CM and C2 ungrouped) by phyllosilicate fraction: PSD-XRD modal mineralogy and planetesimal environments. *Geochim. Cosmochim. Acta* **149**, 206-222, doi:10.1016/j.gca.2014.10.025.
44. Ikeda, Y., (1991). Petrology and mineralogy of the Yamato-82162 chondrite (CI). *Antarc. Met. Res.* **4**, 187-225.
45. Ikeda, Y., (1992). An overview of the research consortium, Antarctic carbonaceous chondrites with CI affinities, Yamato-86720, Yamato-82162, and Belgica-7904". *Antarc. Met. Res.* **5**, 49-73.
46. Ivanova, M.A., Nazarov, M.A., Brandstätter, F., Moroz, L.V., Ntaflos, T. and Kurat, G., (2005). Mineralogical differences between metamorphosed and non-metamorphosed CM chondrites. 36th Lunar and Planetary Science Conference (Abstr.#1054).
47. Ivanova, M.A., Lorenz, C.A., Nazarov, M.A., Brandstaetter, F., Franchi, I.A., Moroz, L.V., Clayton, R.N. and Bychkov, A.Y., (2010). Dhofar 225 and Dhofar 735: Relationship to CM2 chondrites and metamorphosed carbonaceous chondrites, Belgica-7904 and Yamato-86720. *Meteorit. Planet. Sci.* **45**, 1108-1123, doi:10.1111/j.1945-5100.2010.01064.x.
48. Ivanova, M.A., Lorenz, C.A., Franchi, I.A., Bychkov, A.Y. and Post, J.E., (2013). Experimental simulation of oxygen isotopic exchange in olivine and implication for the formation of metamorphosed carbonaceous chondrites. *Meteorit. Planet. Sci.* **48**, 2059-2070, doi:10.1111/maps.12204.
49. Jarosewich, E., Nelen, J.A., Norberg, J.A., (1980). Reference samples for electron microprobe analysis. *Geostand. Newsl.* **4**, 43-47, doi:10.1111/j.1751-908X.1980.tb00273.x.
50. Jilly-Rehak, C.E., Huss, G.R., Nagashima, K. and Schrader, D.L., (2018). Low-temperature aqueous alteration on the CR chondrite parent body: Implications from in situ oxygen-isotope analyses. *Geochim. Cosmochim. Acta* **222**, 230-252, doi:10.1016/j.gca.2017.10.007.
51. Karunadasa, K.S., Manoratne, C.H., Pitawala, H.M.T.G.A. and Rajapakse, R.M.G., (2019). Thermal decomposition of calcium carbonate (calcite polymorph) as examined by in-situ high-temperature X-ray powder diffraction. J. Phys. Chem. Solid. **134**, 21-28, doi:10.1016/j.jpcs.2019.05.023.

52. Keller, L.P. and Buseck, P.R., (1990). Aqueous alteration in the Kaba CV3 carbonaceous chondrite. *Geochim. Cosmochim. Acta* **54**, 2113-2120, doi:10.1016/0016-7037(90)90274-O.
53. Kikuchi, K., Nakamura, T., Nakashima, D., Nagao, K., Imae, N., Yamaguchi, A. and Kojima, H., (2015). Yamato-980115: CI chondrite experienced incomplete dehydration deduced from mineralogy and noble gas signatures. *8th Kaikyokuiki Science Symposium*.
54. Kimura, M., Grossman, J.N. and Weisberg, M.K., (2011). Fe-Ni metal and sulfide minerals in CM chondrites: An indicator for thermal history. *Meteorit. Planet. Sci.* **46**, 431-442, doi:10.1111/j.1945-5100.2010.01164.x.
55. King, A.J., Schofield, P.F., Howard, K.T. and Russell, S.S., (2015a). Modal mineralogy of CI and CI-like chondrites by X-ray diffraction. *Geochim. Cosmochim. Acta* **165**, 148-160, doi:10.1016/j.gca.2015.05.038.
56. King, A.J., Solomon, J.R., Schofield, P.F. and Russell, S.S., (2015b). Characterising the CI and CI-like carbonaceous chondrites using thermogravimetric analysis and infrared spectroscopy. Earth, Planets Space **67**, 1-12, doi:10.1186/s40623-015-0370-4.
57. King, A.J., Schofield, P.F. and Russell, S.S., (2017). Type 1 aqueous alteration in CM carbonaceous chondrites: Implications for the evolution of water-rich asteroids. *Meteorit. Planet. Sci.* **52**, 1197-1215, doi:10.1111/maps.12872.
58. King, A.J., Bates, H.C., Krietsch, D., Busemann, H., Clay, P.L., Schofield, P.F. and Russell, S.S., (2019). The Yamato-type (CY) carbonaceous chondrite group: Analogues for the surface of asteroid Ryugu? *Geochemistry*, doi:10.1016/j.chemer.2019.08.003.
59. Kohobhange S.P., Karunadasa, K.S., Manoratne, C.H., Pitawala, H.M.T.G.A. and Rajapakse, R.M.G., (2019). Thermal decomposition of calcium carbonate (calcite polymorph) as examined by in-situ high-temperature X-ray powder diffraction. J. Phys. Chem. Solid. **134**, 21-28, doi:10.1016/j.jpcs.2019.05.023.
60. Lauretta, D.S., Hua, X. and Buseck, P.R., (2000). Mineralogy of fine-grained rims in the ALH 81002 CM chondrite. *Geochim. Cosmochim. Acta* **64**, 3263-3273, doi:10.1016/S0016-7037(00)00425-7.
61. Llana-Fúnez, S., Brodie, K.H., Rutter, E.H. and Arkwright, J.C., (2007). Experimental dehydration kinetics of serpentinite using pore volumometry. *J. Metamor. Geology* **25**, 423-438, doi:10.1111/j.1525-1314.2007.00703.x.
62. Le Guillou, C. and Brearley, A., (2014). Relationships between organics, water and early stages of aqueous alteration in the pristine CR3. 0 chondrite MET 00426. *Geochim. Cosmochim. Acta* **131**, 344-367, doi:10.1016/j.gca.2013.10.024.
63. Lee, M.R. and Bland, P.A., (2004). Mechanisms of weathering of meteorites recovered from hot and cold deserts and the formation of phyllosilicates. *Geochim. Cosmochim. Acta* **68**, 893-916, doi: 10.1016/S00167037(03)00486-1.
64. Lee, M.R., Lindgren, P., Sofe, M.R., Alexander, C.O.D. and Wang, J., (2012). Extended chronologies of aqueous alteration in the CM2 carbonaceous chondrites: Evidence from carbonates in Queen Alexandra Range 93005. *Geochim. Cosmochim. Acta* **92**, 148-169, doi:10.1016/j.gca.2012.06.005.
65. Lee, M.R., Sofe, M.R., Lindgren, P., Starkey, N.A. and Franchi, I.A., (2013). The oxygen isotope evolution of parent body aqueous solutions as recorded by multiple carbonate generations in the Lonewolf Nunataks 94101 CM2 carbonaceous chondrite. *Geochim. Cosmochim. Acta* **121**, 452-466, doi:10.1016/j.gca.2013.07.010.
66. Lee, M.R., Lindgren, P. and Sofe, M.R., (2014). Aragonite, breunnerite, calcite and dolomite in the CM carbonaceous chondrites: High fidelity recorders of progressive parent body aqueous alteration. *Geochim. Cosmochim. Acta* **144**, 126-156, doi:10.1016/j.gca.2014.08.019.
67. Lindgren, P., Hanna, R.D., Dobson, K.J., Tomkinson, T. and Lee, M.R., (2015). The paradox between low shock-stage and evidence for compaction in CM carbonaceous chondrites explained by multiple low-intensity impacts. *Geochim. Cosmochim. Acta* **148**, 159-178, doi:10.1016/j.gca.2014.09.014
68. Lindgren, P., Lee, M.R., Starkey, N.A. and Franchi, I.A., (2017). Fluid evolution in CM carbonaceous chondrites tracked through the oxygen isotopic compositions of carbonates. *Geochim. Cosmochim. Acta* **204**, 240-251, doi:10.1016/j.gca.2017.01.048.
69. Lipschutz, M.E., Zolensky, M.E. and Bell, M.S., (1999). New petrographic and trace element data on thermally metamorphosed carbonaceous chondrites. *Antarc. Met. Res.* **12**, 57-80.
70. Matsuoka, K., Nakamura, T., Nakamuta, Y. and Takaoka, N., (1996). Yamato-86789: A heated CM-like carbonaceous chondrite. *Antarc. Met. Res.* **9**, 20-36.

71. Nakamura, T., (2005). Post-hydration thermal metamorphism of carbonaceous chondrites. *J. Mineralog. Petrolog. Sci.* **100**, 260-272, doi:10.2465/jmps.100.260
72. Nakamura, T., (2006). Yamato 793321 CM chondrite: Dehydrated regolith material of a hydrous asteroid. *Earth Planet. Sci. Lett.* **242**, 26-38, doi:10.1016/j.epsl.2005.11.040.
73. Nakato, A., Nakamura, T., Kitajima, F. and Noguchi, T., (2008). Evaluation of dehydration mechanism during heating of hydrous asteroids based on mineralogical and chemical analysis of naturally and experimentally heated CM chondrites. *Earth, Planet. Space* **60**, 855-864, doi:10.1186/BF03352837.
74. Nozaki, W., Nakamura, T. and Noguchi, T., (2006). Bulk mineralogical changes of hydrous micrometeorites during heating in the upper atmosphere at temperatures below 1000ºC. *Meteorit. Planet. Sci.* **41**, 1095-1114, doi:10.1111/j.1945-5100.2006.tb00507.x.
75. Ohnishi, I. and Tomeoka, K., (2007). Hydrothermal alteration experiments of enstatite: implications for aqueous alteration of carbonaceous chondrites. *Meteorit. Planet. Sci.* **42**, 49-61, doi:10.1111/j.1945-5100.2007.tb00217.x.
76. Paul, R.L. and Lipschutz, M.E., (1990). Consortium study of labile trace elements in some Antarctic carbonaceous chondrites: Antarctic and non-Antarctic meteorite comparisons. *Antarc. Met. Res.* **3**, 80.
77. Pignatelli, I., Marrocchi, Y., Vacher, L.G., Delon, R. and Gounelle, M., (2016). Multiple precursors of secondary mineralogical assemblages in CM chondrites. *Meteorit. Planet. Sci.* **51**, 785-805, doi:10.1111/maps.12625.
78. Ptáček, P., Šoukal, F. and Opravil, T., (2017). Kinetics and mechanism of thermal decomposition of calcite and aragonite. *J. Met. Mater. Miner.* **3**, 71-79, doi:10.1016/j.jpcs.2019.05.023.
79. Quirico, E., Orthous-Daunay, F.R., Beck, P., Bonal, L., Brunetto, R., Dartois, E., Pino, T., Montagnac, G., Rouzaud, J.N., Engrand, C. and Duprat, J., (2014). Origin of insoluble organic matter in type 1 and 2 chondrites: New clues, new questions. *Geochim. Cosmochim. Acta* **136**, 80-99, doi:10.1016/j.gca.2014.03.025.
80. Quirico, E., Bonal, L., Beck, P., Yabuta, H., Nakamura, T., Nakato, A., Flandinet, L., Montagnac, G., Schmitt-Kopplin, P. and Herd, C.D.K., (2018). Prevalence and nature of heating processes in CM and C2-ungrouped chondrites as revealed by insoluble organic matter. *Geochim. Cosmochim. Acta* **241**, 17-37, doi:10.1016/j.gca.2018.08.029.
81. Rosenberg, N.D., Browning, L. and Bourcier, W.L., (2001). Modeling aqueous alteration of CM carbonaceous chondrites. *Meteorit. Planet. Sci.* **36**, 239-244, doi:10.1111/j.1945-5100.2001.tb01868.x.
82. Russell, S.S., Zolensky, M., Righter, K., Folco, L., Jones, R., Connolly Jr, H.C., Grady, M.M. and Grossman, J.N., (2005). The meteoritical bulletin, no. 89, 2005 September. *Meteorit. Planet. Sci.* **40**, A201-A263, doi:10.1111/j.1945-5100.2005.tb00425.x.
83. Salvador, A.R., Calvo, E.G. and Aparicio, C.B., (1989). Effects of sample weight, particle size, purge gas and crystalline structure on the observed kinetic parameters of calcium carbonate decomposition. *Thermochim. Acta* **143**, 339-345, doi:10.1016/0040-6031(89)85073-7.
84. Schofield, P.F., Knight, K.S., Covey-Crump, S.J., Cressey, G. and Stretton, I.C., (2002). Accurate quantification of the modal mineralogy of rocks when image analysis is difficult. *Miner. Mag.* **66**, 189-200, doi:10.1180/0026461026610022.
85. Skirius, C., Steele, I.M. and Smith, J.V., (1986). Belgica-7904: A new carbonaceous chondrite from Antarctica; Minor element chemistry of olivine. *Memoirs of National Institute of Polar Research. Special issue* **41**, 243-258.
86. Suttle, M.D., Genge, M.J., Folco, L. and Russell, S.S., (2017). The thermal decomposition of fine-grained micrometeorites, observations from mid-IR spectroscopy. *Geochim. Cosmochim. Acta* **206**, 112-136, doi:10.1016/j.gca.2017.03.002.
87. Suttle, M.D., Folco, L., Genge, M.J., Russell, S.S., Najorka, J. and van Ginneken, M., (2019). Intense aqueous alteration on C-type asteroids: Perspectives from giant fine-grained micrometeorites. *Geochim. Cosmochim. Acta* **245**, 352-373, doi:10.1016/j.gca.2018.11.019.
88. Suttle, M.D., Dionnet, Z., Franchi, I., Folco, L., Gibson, J., Greenwood, R.C., Rotundi, A., King, A. and Russell, S.S., (2020). Isotopic and textural analysis of giant unmelted micrometeorites–identification of new material from intensely altered 16O-poor water-rich asteroids. *Earth Planet. Sci. Lett.* **546**, doi:10.1016/j.epsl.2020.116444.

89. The Meteoritical Bulletin (2020), online and available at:https://www.lpi.usra.edu/meteor/ (accessed on 28/04/2020).
90. Tomeoka, K., (1990). Mineralogy and petrology of Belgica-7904: A new kind of carbonaceous chondrite from Antarctica. *Antarc. Met. Res.* **3**, 40-54.
91. Tomeoka, K. and Buseck, P.R., (1988). Matrix mineralogy of the Orgueil CI carbonaceous chondrite. *Geochim. Cosmochim. Acta* **52**, 1627-1640, doi:10.1016/0016-7037(88)90231-1.
92. Tomeoka, K. and Buseck, P.R., (1990). Phyllosilicates in the Mokoia CV carbonaceous chondrite: Evidence for aqueous alteration in an oxidizing environment. *Geochim. Cosmochim. Acta* **54**, 1745-1754, doi:10.1016/0016-7037(90)90405-A.
93. Tomeoka, K., Kojima, H. and Yanai, K., (1989a). Yamato-82162: A new kind of CI carbonaceous chondrite found in Antarctica. *Antarc. Met. Res.* **2**, 36-54
94. Tomeoka, K., Kojima, H. and Yanai, K., (1989b). Yamato-86720: A CM carbonaceous chondrite having experienced extensive aqueous alteration and thermal metamorphism. *Antarc. Met. Res.* **2**, 55-74
95. Tomeoka, K., McSween Jr, H.Y. and Buseck, P.R., (1989c). Mineralogical alteration of CM carbonaceous chondrites: A review. *In Proc. NIPR Symp. Antarct. Meteorites* **2**, 221-234.
96. Tomkins, A.G., (2009). What metal-troilite textures can tell us about post-impact metamorphism in chondrite meteorites. *Meteorit. Planet. Sci.* ***44***, 1133-1149, doi:10.1111/j.1945-5100.2009.tb01213.x.
97. Tonui, E., Zolensky, M. and Lipschutz, M., (2002). Petrography, mineralogy and trace element chemistry of Yamato-86029 Yamato-793321 and Lewis Cliff 85332: Aqueous alteration and heating events. *Antarc. Met. Res.* **15**, 38-58.
98. Tonui, E., Zolensky, M., Hiroi, T., Nakamura, T., Lipschutz, M.E., Wang, M.S. and Okudaira, K., (2014). Petrographic, chemical and spectroscopic evidence for thermal metamorphism in carbonaceous chondrites I: CI and CM chondrites. *Geochim. Cosmochim. Acta* **126**, 284-306, doi:10.1016/j.gca.2013.10.053.
99. Vacher, L.G., Truche, L., Faure, F., Tissandier, L., Mosser-Ruck, R. and Marrocchi, Y., (2019a). Deciphering the conditions of tochilinite and cronstedtite formation in CM chondrites from low temperature hydrothermal experiments. *Meteorit. Planet. Sci.* **54**, 1870-1889, doi:10.1111/maps.13317.
100. Vacher, L.G., Piralla, M., Gounelle, M., Bizzarro, M. and Marrocchi, Y., (2019b). Thermal evolution of hydrated asteroids inferred from oxygen isotopes. *Astrophys. J. Lett.* **882**, L20.
101. Valverde, J.M., Perejon, A., Medina, S. and Perez-Maqueda, L.A., (2015). Thermal decomposition of dolomite under CO 2: insights from TGA and in situ XRD analysis. Phys. Chem. Chem. Phys. **17**, 30162-30176, doi:10.1039/C5CP05596B.
102. van Schmus, W.R. and Wood, J.A., (1967). A chemical-petrologic classification for the chondritic meteorites. Geochim. Cosmochim. Acta **31**, 747-765, doi:10.1016/S0016-7037(67)80030-9.
103. Velbel, M.A., Tonui, E.K. and Zolensky, M.E., (2012). Replacement of olivine by serpentine in the carbonaceous chondrite Nogoya (CM2). *Geochim. Cosmochim. Acta* **87**, 117-135, doi:10.1016/j.gca.2012.03.016.
104. Verdier-Paoletti, M.J., Marrocchi, Y., Vacher, L.G., Gattacceca, J., Gurenko, A., Sonzogni, C. and Gounelle, M., (2019). Testing the genetic relationship between fluid alteration and brecciation in CM chondrites. *Meteorit. Planet. Sci.*, 54, 1692-1709, doi:10.1111/maps.13306.
105. Weisberg, M.K., McCoy, T.J. and Krot, A.N., 2006. Systematics and evaluation of meteorite classification. Meteorites and the early solar system II.
106. Wendt, M. and Schmidt, A., (1978). Improved reproducibility of energy-dispersive X-ray microanalysis by normalization to the background. *physica status solidi (a)*, 46:179-183, doi:10.1002/pssa.2210460121.
107. Wogelius, R.A. and Walther, J.V., (1992). Olivine dissolution kinetics at near-surface conditions. *Chem. Geol.* **97**, 101-112, doi:10.1016/0009-2541(92)90138-U.
108. Yamamoto, K. and Nakamura, N., (1990). REE characteristics of Yamato-82162 and-86720 meteorites and their inference to classification. Antar. Met. Res. **3,** 69-79.
109. Yoder, H.S. and Eugster, H.P., (1954). Phlogopite synthesis and stability range. *Geochim. Cosmochim. Acta* **6**, 157-185, doi:10.1016/0016-7037(54)90049-6.
110. Zolensky, M.E., (1984). Hydrothermal alteration of CM carbonaceous chondrites; implications of the identification of tochilinite as one type of meteoritic PCP. *In 47th Annual Meeting of the Meteoritical Society* (Vol. 537, p. 19).

111. Zolensky, M.E. and Mackinnon, I.D., (1986). Microstructures of cylindrical tochilinites. *Amer. Miner.* **71**, 1201-1209.
112. Zolensky, M., Barrett, R. and Browning, L., (1993). Mineralogy and composition of matrix and chondrule rims in carbonaceous chondrites. *Geochim. Cosmochim. Acta* **57**, 3123-3148, doi:10.1016/0016-7037(93)90298-B.
113. Zolensky, M.E., Nakamura, K., Gounelle, M., Mikouchi, T., Kasama, T., Tachikawa, O. and Tonui, E., (2002). Mineralogy of Tagish Lake: An ungrouped type 2 carbonaceous chondrite. *Meteorit. Planet. Sci.* **37**, 737-761, doi:10.1111/j.1945-5100.2002.tb00852.x.
114. Zolotov, M.Y., Mironenko, M.V. and Shock, E.L., (2006). Thermodynamic constraints on fayalite formation on parent bodies of chondrites. *Meteorit. Planet. Sci.* **41**, 1775-1796, doi:10.1111/j.1945-5100.2006.tb00451.x.
115. Zolotov, M.Y., (2012). Aqueous fluid composition in CI chondritic materials: Chemical equilibrium assessments in closed systems. *Icarus* **220**, 713-729, doi:10.1016/j.icarus.2012.05.036.

List of Figures and Tables:

Table.1. Physical, chemical and mineralogical properties of CY meteorites (and potential CY meteorites). Data taken from the literature: *this study, [a.]Bischoff and Metzler, 1991, [b.]Tomeoka et al., 1989b, [c.]Lipschutz et al., 1999, [d.]Matsuoka et al., 1996, [e.]Ivanova et al., 2010, [f.]Bouvier et al., 2017b, [g.]Gattacceca et al., 2019, [h.]Bouvier et al., 2017a, [i.]Braukmüller et al., 2018, [j.]King et al., 2019, [k.]Tomeoka et al., 1989a, [L.]Haramura et al., 1983, [m.]King et al., 2015a.

	Chondrule size *(μm)*			***Chondrule + CAI abundance***	***H_2O***	***Recons. Phyllo.*** *(vol%)*	***Sulfid.*** *(vol%)*	***Met. Bul. Classific.***	***Pairing***
Sample	***Min***	***Max***	***Avg.***	*(area%)*	*(wt.%)*				
Y-82162	*No chondrules/CAIs preserved (replaced by aqueous alteration)*				11.9[k]	79[m]	19[n]	C1/2-ung	
Y-980115						79[m]	19[n]	CI1	
Y-86029						76[j]	19[j]	CI1	
Y-86720	100[b]	1500[c]		10.6[b]-13[a]	6.3[b]	58[j]	29[j]	C2-ung	Pairing suggested
Y-86789	600[d]	750[d]		14[d]	<5[d]	63[j]	28[j]	C2-ung	
B-7904	500[a]	3000[a]		18[a]	2.6[L]	61[j]	12[j]	C2-ung	
Dho 735	100[e]	800[e]	350[e]		1.06[e]			CM2	Pairing suggested
Dho 2066	340[g]	900[g]	620[g]					C-ung	
Dho 1988			530*-550[f]					C2-ung	
Dho 225			330[e]	26[e]	1.76[e]			CM-an	Pairing suggested, could also include Dho 955?
Dho 2046			240[h]	20[h]				CM2-an	
AVG.			*418*	*18*	*5*	*69*	*21*		

Table.2. Chemical compositions of main phases in Dho 1988, measured by EDS and WDS. Data are expressed in element wt.%. **Note**: some rows are listed as "2nd ol." (secondary olivine). Since solid-state reactions largely preserve the cation composition of their precursor phases the analysis of secondary olivine allows the inferred composition of former phyllosilicates. This is important as it demonstrates two clearly distinct phyllosilicate species used to exist in the former aqueously altered assemblage. The symbol "-"represents analyses with data below detection threshold.

Phase	*Instru.*	*Analysis*	*N=?*	*Na*	*Mg*	*Al*	*Si*	*P*	*S*	*Cl*	*K*	*Ca*	*Ti*	*Cr*	*Mn*	*Fe*	*Ni*	*C*	*O*	*Total*
Primary olivine	*EDS*	*Avg.*	91	0.02	33.47	0.05	19.70	0.01	0.01	0.00	0.01	0.23	0.02	0.18	0.08	2.16	0.03	-	44.67	100.65
		Stdev.		*0.03*	*1.76*	*0.06*	*0.42*	*0.02*	*0.02*	*0.01*	*0.02*	*0.14*	*0.03*	*0.10*	*0.08*	*2.67*	*0.04*	-	*1.52*	*1.73*
Low-Ca px. (enstatite)	*WDS*	*Avg.*	49	0.33	16.67	2.24	18.61	0.28	0.49	-	0.26	0.15	0.23	1.60	0.27	14.32	0.47	-	40.70	96.61
		Stdev.		*0.16*	*1.47*	*0.52*	*1.97*	*0.25*	*0.48*	-	*0.14*	*0.09*	*0.24*	*0.33*	*0.18*	*3.41*	*0.49*	-	*1.93*	*2.13*
2nd ol. (former phyl. Al-poor)	*WDS*	*Avg.*	*21*	0.15	19.03	1.38	18.38	0.04	0.15	-	0.13	0.39	0.07	0.30	0.14	11.35	0.64	-	38.77	90.92
		Stdev.		0.08	3.56	0.14	1.73	0.02	0.11	-	0.08	0.57	0.05	0.22	0.03	3.31	0.65	-	3.09	4.54
2nd ol. former phyl. Al-rich)	*WDS*	*Avg.*	*26*	0.49	15.76	6.89	16.90	0.15	0.29	-	0.28	0.14	0.13	0.36	0.20	14.65	0.07	-	40.93	97.25
		Stdev.		0.14	1.66	2.26	1.73	0.07	0.15	-	0.14	0.24	0.05	0.19	0.03	2.38	0.08	-	1.17	1.43
Chondrule FGRs	*WDS*	*Avg.*	50	0.04	11.46	1.41	13.66	0.05	0.16	-	0.02	0.72	0.06	0.27	0.12	27.77	1.36	-	33.37	90.47
		Stdev.		*0.02*	*1.31*	*0.56*	*1.17*	*0.02*	*0.12*	-	*0.02*	*1.26*	*0.02*	*0.14*	*0.02*	*3.57*	*0.55*	-	*2.24*	*5.30*
Fe-sulfide (troilite)	*EDS*	*Avg.*	*55*	0.04	0.15	0.12	0.22	0.10	35.56	0.01	0.17	0.14	0.05	0.07	0.02	60.35	0.51	-	0.65	98.16
		Stdev.		*0.04*	*0.36*	*0.05*	*0.33*	*0.04*	*1.65*	*0.02*	*0.27*	*0.22*	*0.06*	*0.16*	*0.03*	*2.67*	*1.20*	-	*1.31*	*3.63*
Calcium carbonate	*EDS*	*Avg.*	*16*	0.04	0.56	0.06	0.26	0.07	0.42	0.02	0.02	37.14	0.02	0.02	0.04	0.92	0.07	15.55	44.88	100.09
		Stdev.		*0.05*	*0.19*	*0.05*	*0.35*	*0.06*	*0.22*	*0.03*	*0.02*	*1.28*	*0.02*	*0.03*	*0.06*	*0.96*	*0.08*	*1.87*	*1.71*	*0.08*
Apatite (Plus F: 1.49 ± 0.67)	*EDS*	*Avg.*	*6*	0.02	1.51	0.10	1.59	9.06	0.93	0.51	0.05	34.81	0.03	0.00	0.07	1.20	0.12	-	38.15	89.61
		Stdev.		*0.02*	*0.59*	*0.05*	*0.81*	*4.35*	*0.25*	*0.23*	*0.03*	*1.12*	*0.03*	*0.04*	*0.07*	*0.47*	*0.09*	-	*1.65*	*5.20*
FeCr-sulfide	*EDS*	S1-62	1	0.00	0.00	0.22	0.00	0.00	32.75	0.00	0.00	0.00	0.00	45.80	0.65	13.96	0.00	-	0.00	93.38
Chromite	*EDS*	S2-267	1	0.02	2.69	0.20	0.62	0.02	0.01	0.00	0.01	0.06	0.17	43.97	0.35	20.24	0.00	-	29.04	97.40
Fe-Ni metal (kamacite)	*EDS*	S2-115	1	0.00	0.16	0.08	0.28	0.09	0.00	0.06	0.04	0.25	0.05	0.05	0.00	88.28	7.10	-	0.56	97.00
Fe-Ni metal (taenite)	*EDS*	S2-75	1	0.00	0.04	0.12	0.03	0.08	0.02	0.00	0.03	0.02	0.00	0.08	0.05	46.03	51.34	-	0.66	98.50
Partially alter. metal	*EDS*	S2-279	1	0.00	3.74	0.59	2.48	0.00	0.00	0.00	0.00	0.00	0.20	1.09	0.00	47.48	37.65	-	7.20	100.43
Mg-Ilmenite	*EDS*	S2-262	1	0.07	2.52	0.16	0.29	0.10	0.00	0.00	0.00	0.45	31.86	0.26	0.25	31.78	0.00	-	33.27	101.01

Table.3. X-Ray diffraction modal mineralogy results for Dho 1988.

Phases	***AVG.***	***STDEV.***
Total Ol.	73	3
Secondary Ol.	62	2
Primary Ol.	11	0
Pyroxene	7	4
Phyllosilicate	0	0
Fe-sulphides	14	1
Oxides	0	0
Metal	0	0
Carbonate	5	1

Fig.1. Bulk O-isotope compositions of CY chondrites and comparison against closely related carbonaceous chondrites (CO, CI and CM chondrites). Note that the CY chondrites plot as an extension of the CO-CM mixing line but at heavier (^{16}O-poor) compositions. Also shown is a single giant unmelted micrometeorite [TAM50-25] whose anomalously heavy O-isotope composition also extends the CM mixing line. Data were taken from: Clayton and Mayeda (1999), Ivanova et al., (2010), Bouvier et al., (2017a; 2017b), Gattacceca et al., (2019) and Suttle et al., (2020).

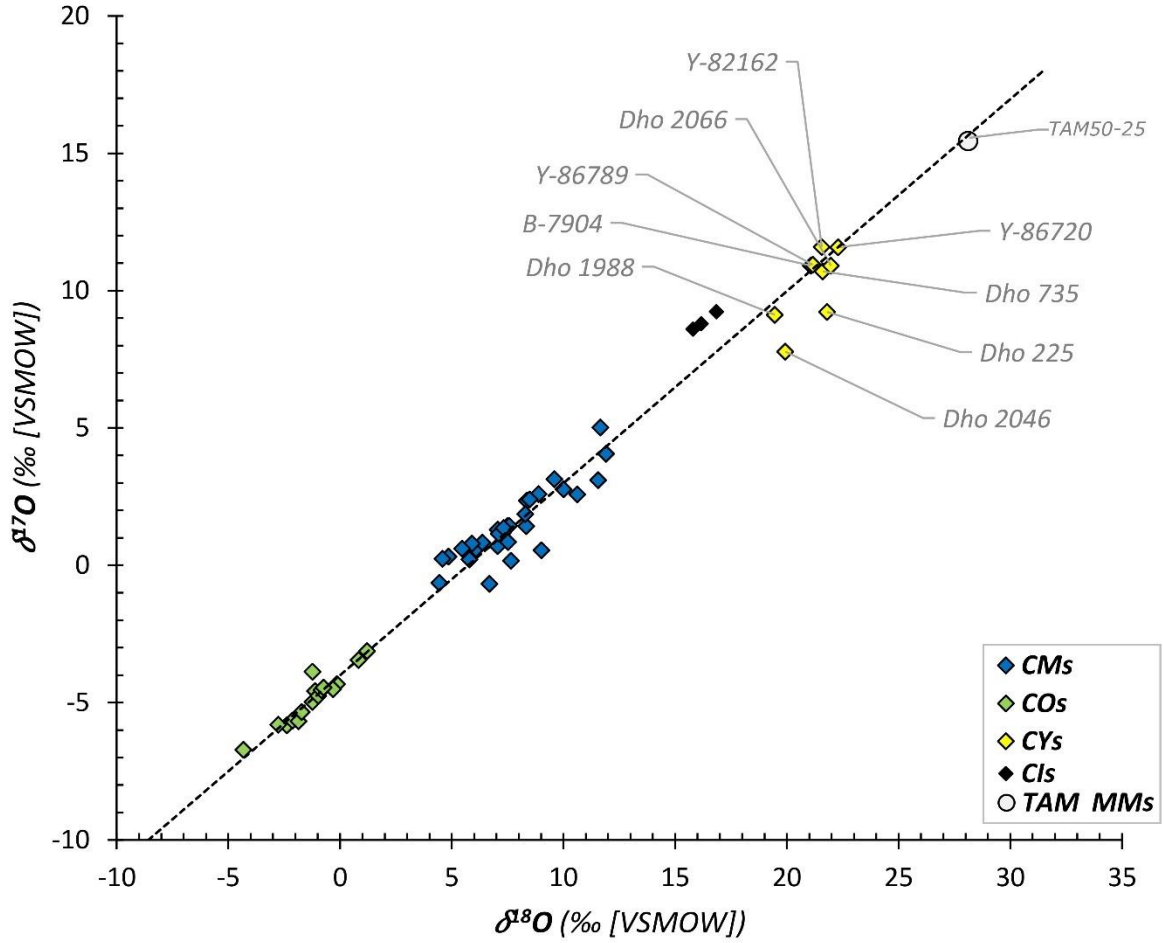

Fig.2. Overview of Dho 1988. (A-C) Combined BSE and EDS maps collected on thin section MNB-XV-II-36, showing relative abundances of (A) major cations, (B) major anions and (C) refractory elements. (D) Interpretative sketch of the section illustrating the positions of chondrules, CAIs, matrix, clasts and veins.

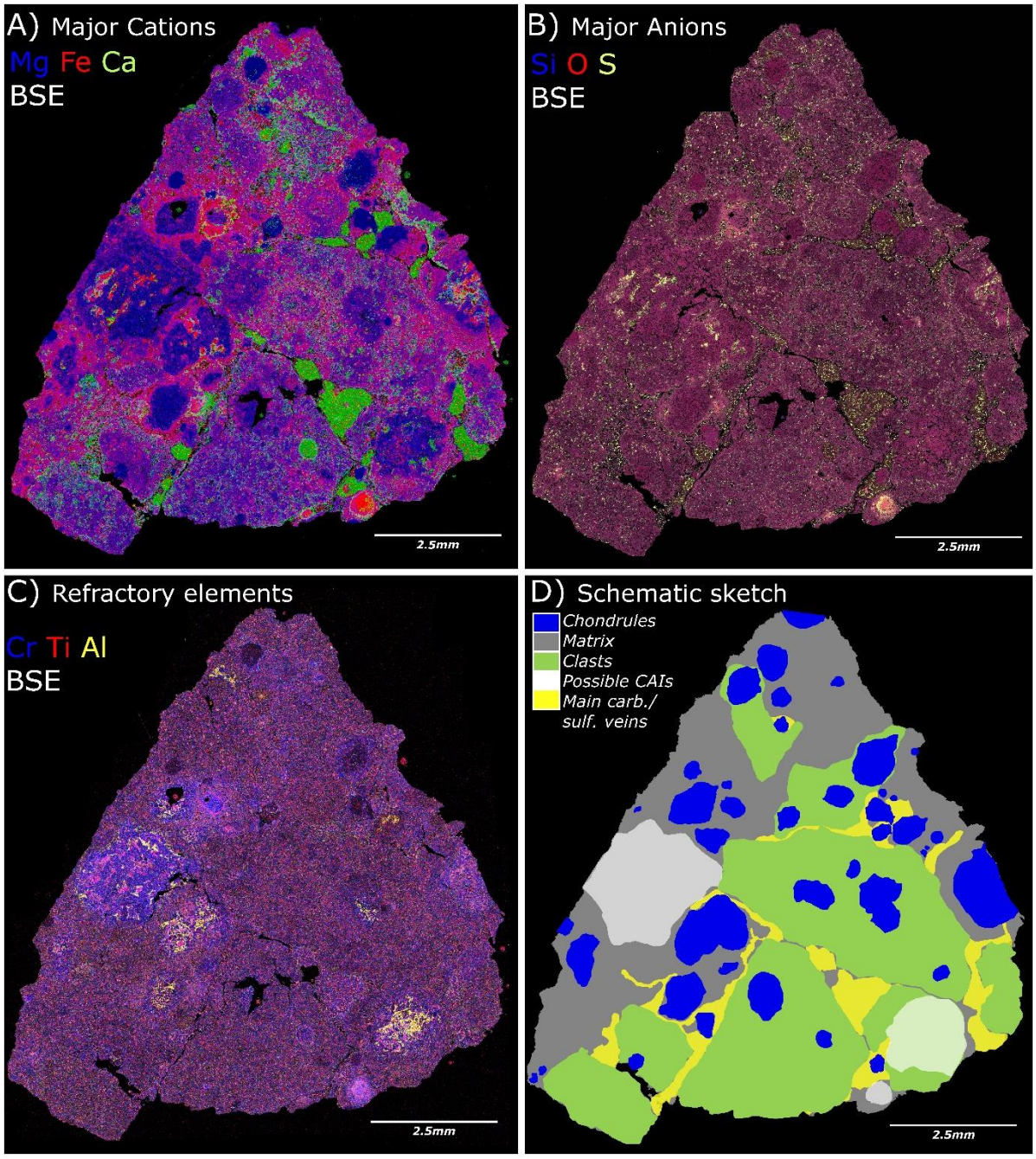

Fig.3. Chondrules in Dho 1988. A & B) Minimally altered chondrules, retaining much of their primary mafic silicates. C) A POP chondrule in which the glassy matrix has been replaced by phyllosilicate (later converted to secondary olivine during metamorphism) while the crystalline anhydrous silicates survived unaltered. D) A heavily altered chondrule in which much of the anhydrous silicate material has been replaced by phyllosilicate. This chondrule has an "armoured" texture characteristised by an outer mantle of Fe-sulphides. Armoured chondrules are common in CYs, reflecting their high sulphur abundances. E) A pseudomorphic chondrule replaced by phyllosilicates. These later dehydrated to produce aligned dehydration cracks, some of which have been infilled by Fe-sulphides. F) A pseudomorphic chondrule in which the secondary phases are sulphides and Ca-carbonates. This is an atypical form of replacement but has been observed in CM chondrites (e.g. Lee et al., 2014).

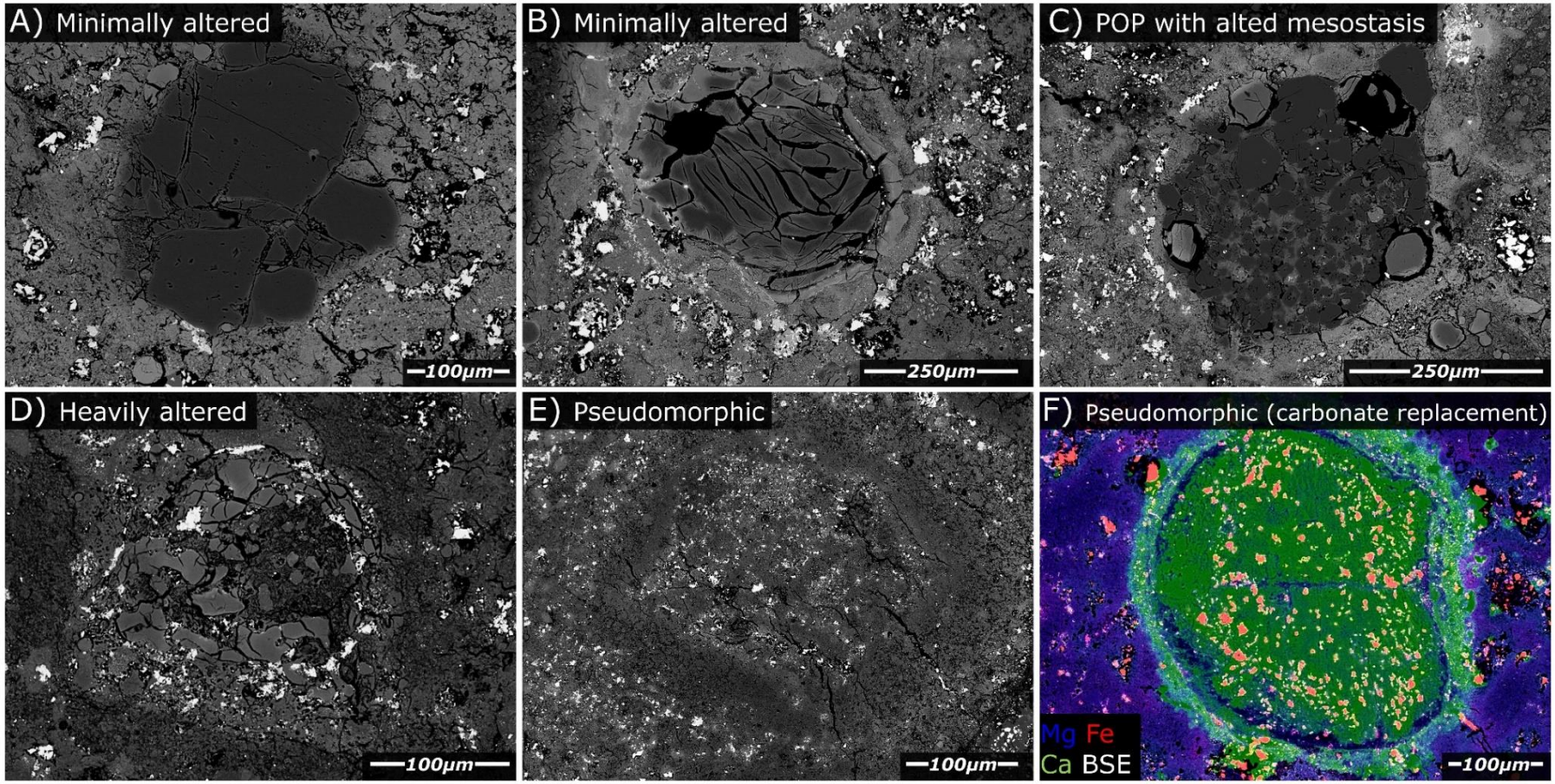

Fig.4. Geochemical data from (A) primary olivine (histogram) and (B-C) secondary olivine within Dho 1988 (allowing the compositions of former phyllosilicates to be inferred). B) Ternary cation compositions and C) identification of the two (former) phyllosilicate species. Note, the presence of Ni detected in some (former) phyllosilicate analyses likely reflects the presence of small Ni-bearing sulphides intermixed in the analysis region. Their presence supports the interpretation that Dho 1988 previously contained TCIs.

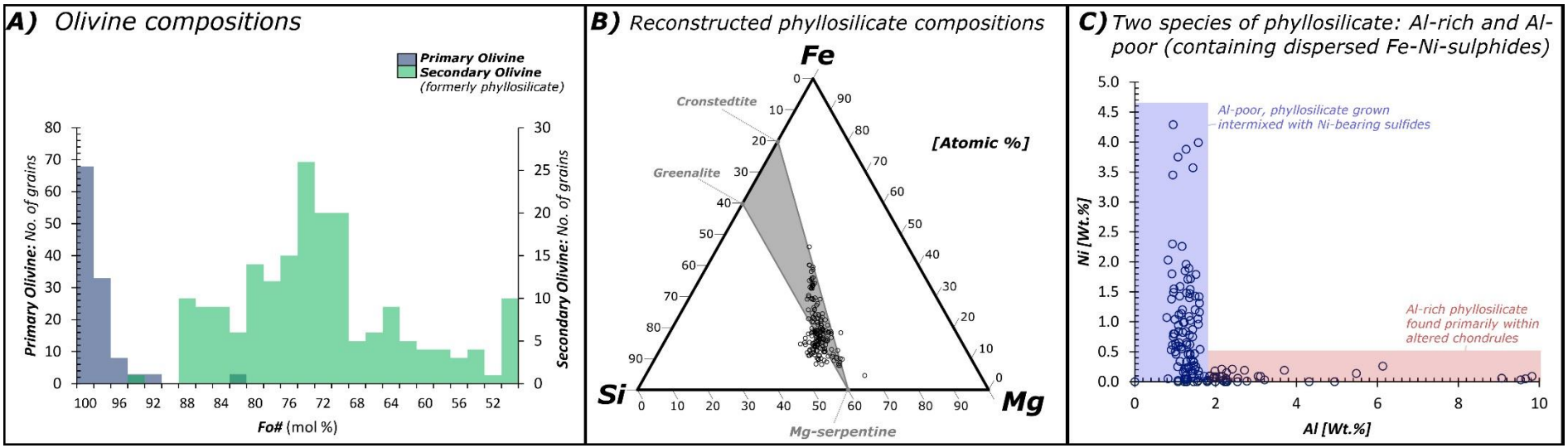

Fig.5.Textural relationships and phases in Dho 1988. A) Dho 1988 is a highly brecciated meteorite, fractures appear as infilled veins composed primarily of carbonate with embedded sulphide. However, dark porosity margins, interpreted as (former) phyllosilicates grew as the first phase during vein precipitation. B) Small matrix-hosted carbonate veins are also common in Dho 1988. C) Within the carbonate-sulphide veins, localised poorly-developed apatite are found. D and E) In aqueously altered chondrule cores, (former) coarse-grained (Al-rich) phyllosilicates are common. They have overgrowths of refractory oxides [Cr-spinel and Mg-ilmenite] indicating late-stage precipitation of oxides onto phyllosilicates. Since dehydration cracks cut the overgrowth rims, the refractory silicates were deposited prior to thermal metamorphism. F) Fine-grained phyllosilicate textures are common within the matrix of Dho 1988. These relict textures are preserved in recrystallized metamorphic groundmass. G) An aqueously altered chondrule pseudomorph. During thermal metamorphism phyllosilicates experienced dehydration, forming cracks which were later infilled by troilite. H & I) In Dho 1988 Fe-metal and troilite co-exist, magnetite is absent.

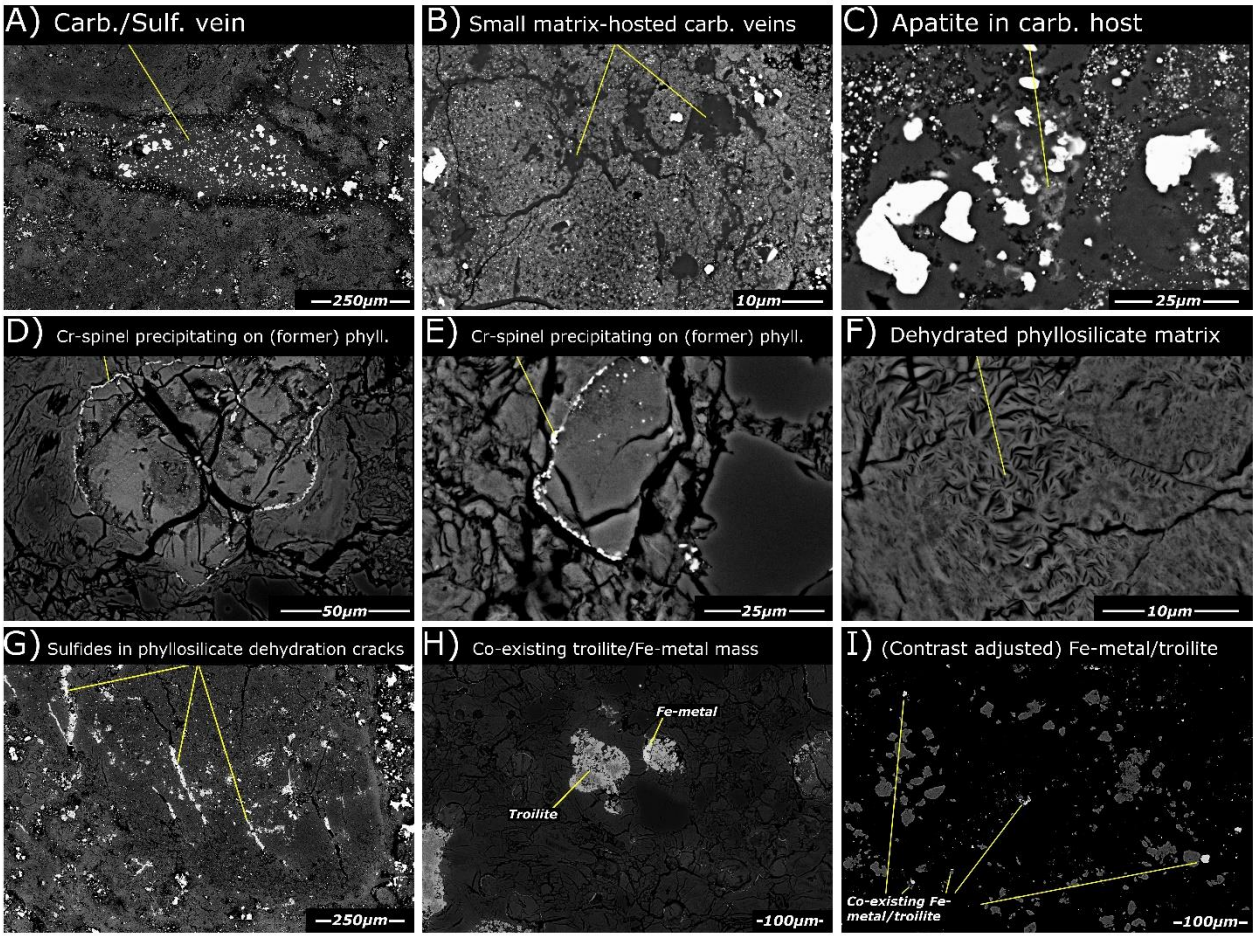

Fig.6. X-ray diffraction pattern for Dho 1988 shown alongside the calculated model pattern and the four-component mineral groups (that make up this model [Ol. = olivine; Sul. = sulphide – specifically troilite; Car. = carbonate, specifically calcite and Px. = pyroxene]). The residual (actual-model), shown in red reflects the model's uncertainty. This model is produced by the pattern stripping process as described in Schofield et al., (2002), Howard et al., (2009) and others.

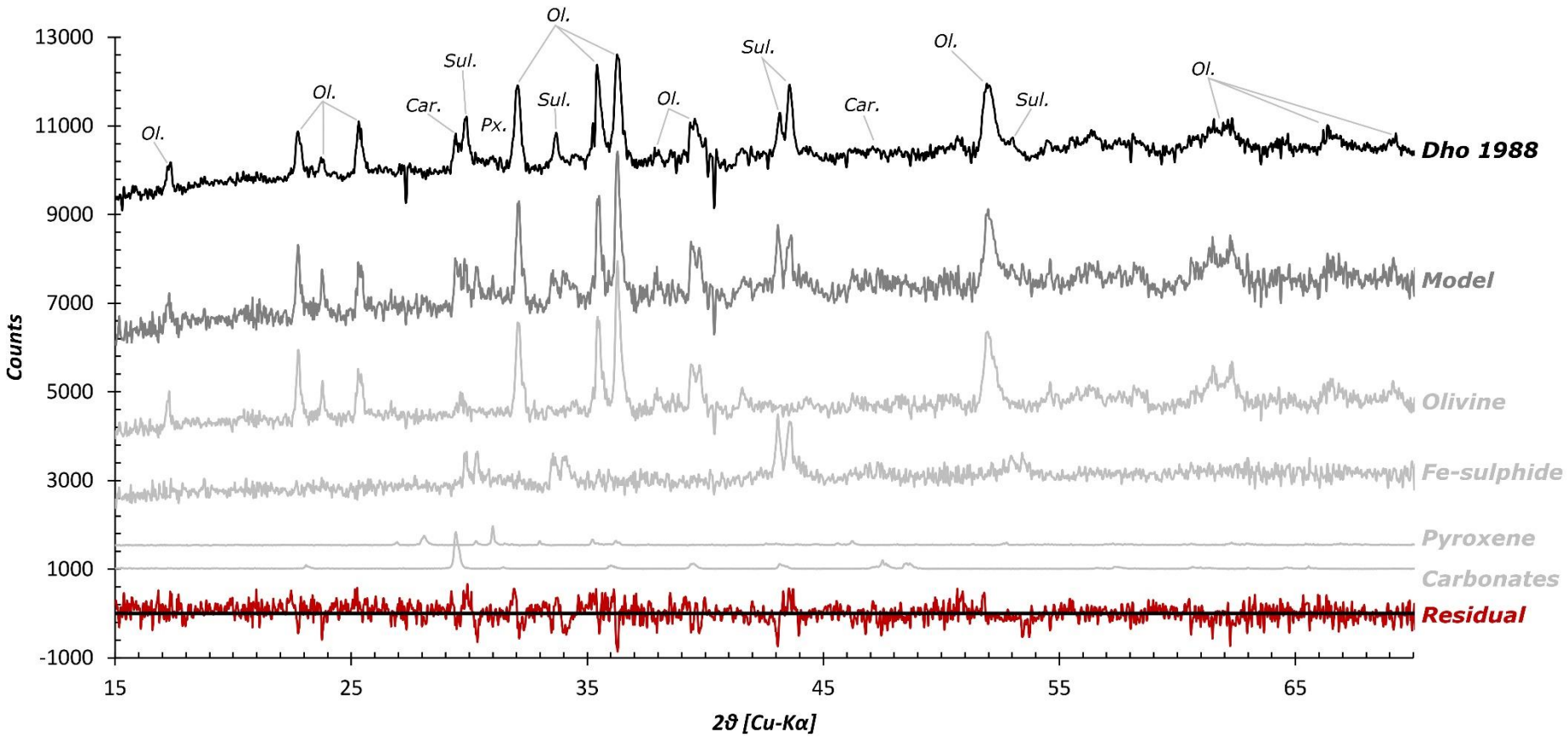

Fig.7. Mass loss (grey) and DTG (black) curves for Dho 1988 (solid lines) compared against a troilite mineral standard (dashed lines [NHM collection ID: BM1923, 21]). Over the range 200-770°C Dho 1988 experienced a loss of 2.72wt.%, comparatively little when compared to other CM and CY chondrites (e.g. ~10-14wt.% in CMs, Garenne et al., 2014; King et al., 2015b). The close agreement between the two curves demonstrates that the volatile loss in Dho 1988 is at least partially due to the loss of sulphur from troilite, however this can only explain ~0.5wt.% of the total mass loss observed, requiring that an additional mineral is required. The second high temperature peak in the Dho 1988 profile (~660ºC in the DTG curve) is a combination of troilite and calcite decomposition, which account for ~2wt.% of the volatiles lost. Thus, the entire mass loss from Dho 1988 could be explained by sulphide and carbonate decomposition, and although some phyllosilicates have a mass loss event around 400-770C there is no definitive evidence for a mass loss event associated with water released from phyllosilicates by dehydration in this sample. Note the dotted black vertical lines separate the TGA profile into distinct regions (defined by Garenne et al., 2014) that reflect the loss of volatiles from different phases 0-220°C (loss of terrestrial adsorbed water), 200-400°C (water loss from Fe-oxyhydroxides), 400-770°C (water loss from phyllosilicates) and 770-900°C (CO_2 loss from carbonates). These regions are simplifications and ignore the emission from S-bearing minerals, which in CYs are of critical importance.

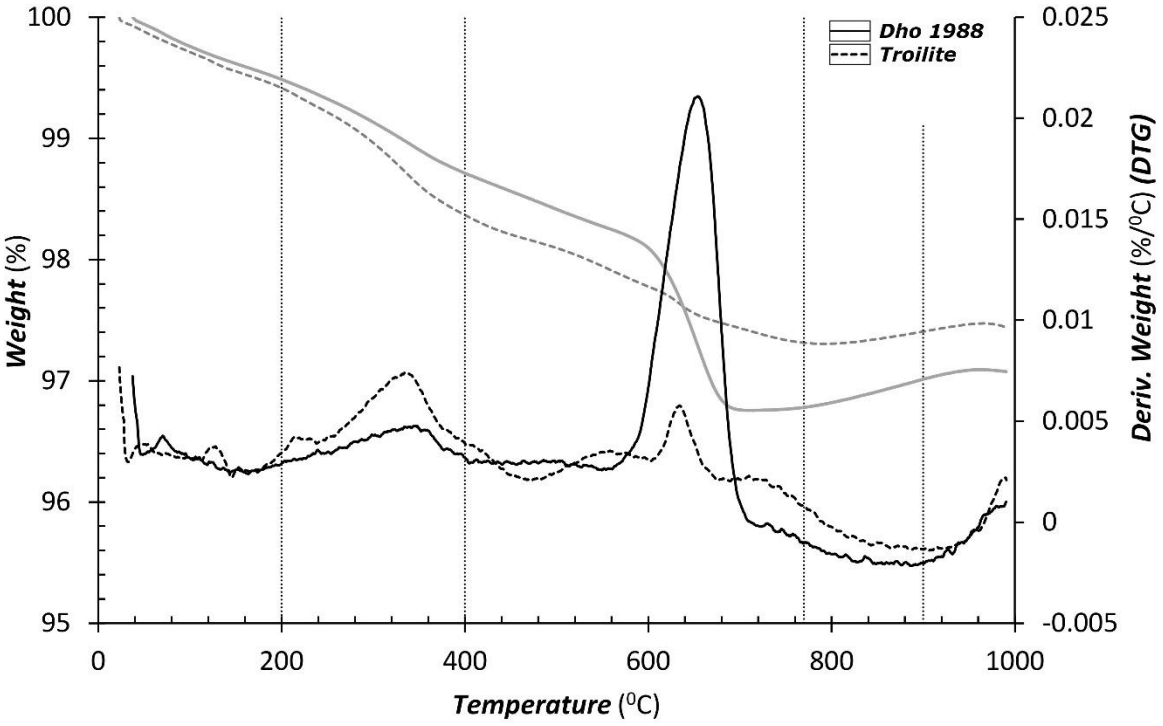

Fig.8. Estimating the degree of aqueous alteration that affected Dho 1988 (prior to later metamorphic overprinting). Evaluated using the scheme of Howard et al., (2015) – based on the relative abundance of secondary olivine (that represents former phyllosilicate) and anhydrous silicate and expressed as a single value the phyllosilicate fraction (PSF). The data for Dho 1988 is given in context, showing previously published data for CM and CR chondrites from Howard et al., (2019), CO chondrites from (Alexander et al., 2018), CY chondrites from King et al., (2019) and non PSD-XRD analysis data from fine-grained micrometeorites (MMs) from the Transantarctic Mountains from Suttle et al., (2019). Note CY chondrite values are labelled.

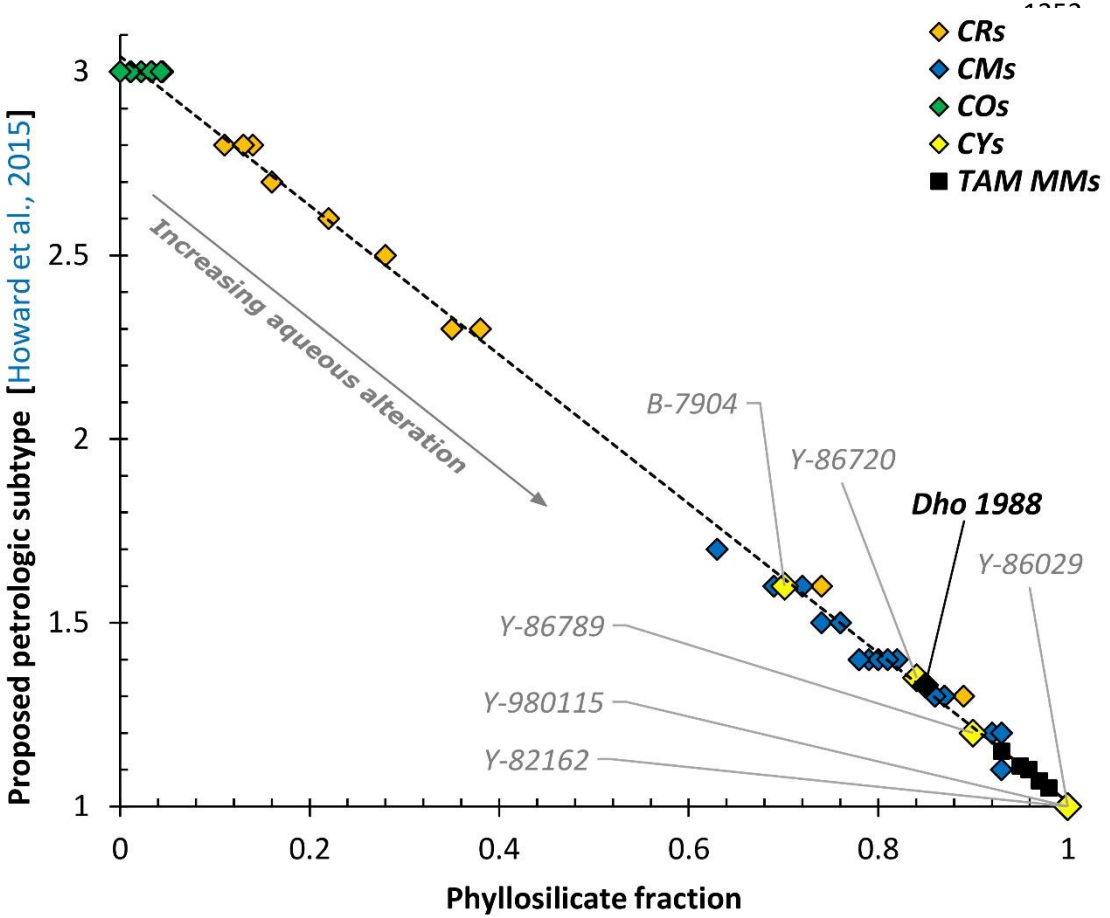

Fig.9. Fugacity-temperature diagram at 1 bar pressure, showing three common buffer assemblages relevant to the Dho 1988 system (iron-wüstite, wüstite-magnetite and Ni-Ni-oxide). The presence of Ni-bearing metal in Dho 1988 (and other CY chondrites)

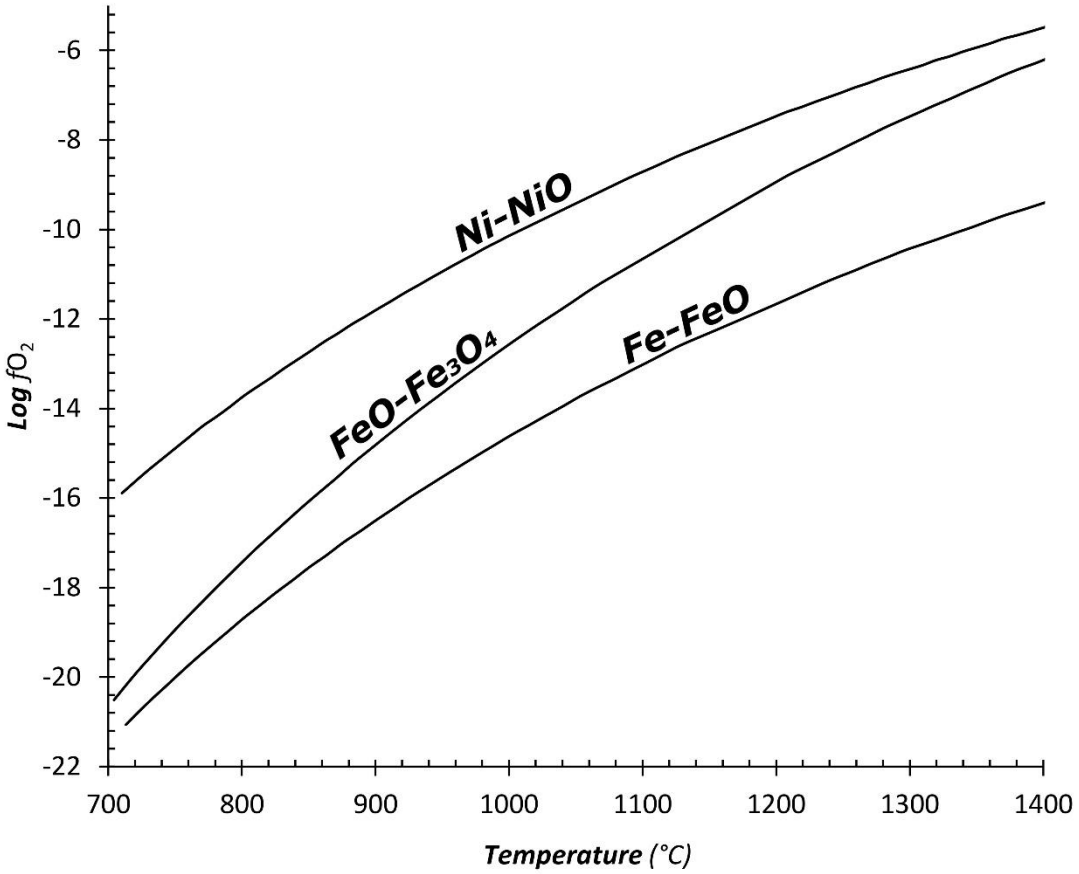

Fig.10. Diagram illustrating the alteration history of Dho 1988. Panel 1 shows an impactor hitting the CY parent body, resulting in brecciation and heating. This impact event may have initiated aqueous alteration or may have occurred during aqueous alteration. In either case, aqueous alteration was active after impact, exploiting the open fractures and precipitating phyllosilicates along fracture walls (panel 2). Panel 2 shows the early stages of aqueous alteration in which TCIs formed, chondrules were altered and magnetite formed by the oxidation of Fe-Ni metal. Panel 3 shows the advanced stages of aqueous alteration in which (some) chondrules were completely altered (forming pseudomorphs), the entire matrix was replaced by phyllosilicates, fractures became infilled by a second later deposit of carbonates plus sulphides and the refractory oxides (Cr-spinel and ilmenite) precipitated on coarse-grained phyllosilicates found in the altered chondrule cores. Panel 4 depicts the effects of thermal metamorphism in which phyllosilicates recrystallize as (secondary) olivine and magnetite is replaced by a second generation of troilite. Carbonates survive heating without decomposing.